AIAA 98-0547

Design of a Mach-6 Quiet-flow Wind-Tunnel Nozzle Using the e**N Method for Transition Estimation

Steven P. Schneider
School of Aeronautics and Astronautics
Purdue University
West Lafayette, IN 47907-1282

36th Aerospace Sciences Meeting & Exhibit
January 12–15, 1998 / Reno, NV

AIAA Paper 98-0547, presented at the Aerospace Sciences Meeting, Jan. 1998, Reno Nevada.
Regenerated in .pdf from original file, Jan. 2003.

Design of a Mach-6 Quiet-Flow Wind-Tunnel Nozzle using the e**N Method for Transition Estimation

Steven P. Schneider*
School of Aeronautics and Astronautics
Purdue University
West Lafayette, IN 47907-1282

Abstract

A high Reynolds-number Mach-6 quiet-flow wind-tunnel nozzle has been designed for a new quiet-flow Ludwieg tube. The quiet-flow nozzle is designed to maintain laminar boundary layers on the nozzle walls as far downstream as possible. A very long nozzle with gentle curvature is used to reduce Görtler instability. Early transition would occur in adiabatic nozzles of this type, due to the first-mode TS instability. This is controlled with an isothermal wall temperature that is high near the throat and tapers to ambient near the exit. The crossflow instability is eliminated through use of an axisymmetric nozzle. Predictions using e^N techniques suggest that a quiet-flow Reynolds number in excess of 13 million can be achieved in a 103-inch-long 9-inch-diameter prototype nozzle at 10 atm. total pressure. This performance would be about twice that of the existing Langley Mach-6 quiet-flow nozzle. A 33-foot-long 24-inch nozzle at the same pressure is predicted to have a quiet Reynolds number of more than 36 million, a value sufficient to allow reproducing many flight experiments.

Introduction

Transition Issues

Laminar-turbulent transition in high-speed boundary layers is important for prediction and control of heat transfer, skin friction, and other boundary layer properties. However, the mechanisms leading to transition are still poorly understood, even in low-noise environments. Applications hindered by this lack of understanding include reusable launch vehicles such as the X-33, high-speed interceptor missiles ([32], [35]), and hypersonic cruise vehicles [1].

The transition process is initiated through the growth and development of disturbances originating on the body or in the freestream [14]. The receptivity mechanisms by which the disturbances enter a boundary layer are influenced by roughness, waviness, bluntness, curvature, Mach number, and so on. The growth of the disturbances is determined by the instabilities of the boundary layer. These instabilities are in turn affected by all the factors determining the mean boundary layer flow, including Mach number, transverse and streamwise curvature, pressure gradient, and temperature [50]. Relevant instabilities include the concave-wall Görtler instability [26], the first and second mode TS-like instability waves described by Mack [38], and the 3D crossflow instability [49]. The first appearance of turbulence is associated with the breakdown of the instability waves, which is determined by various secondary instabilities [29]. Local spots of turbulence grow downstream through an intermittently-turbulent region whose length is dependent on the local flow conditions and on the rate at which spots are generated [45].

In view of the dozens of parameters influencing transition, classical attempts to correlate the general transition 'point' with one or two parameters such as Reynolds number and Mach number can only work for cases that are similar to those previously tested. However, correlations between transition and the integrated growth of the linear instability waves have shown promising agreement with experiment [50]. Although these e^N correlations neglect all receptivity and secondary instability effects, they work fairly well for a variety of conditions where the environmental noise is generally low [41, 48].

Improvements in techniques for estimating the location and extent of transition will depend on

*Associate Professor. Senior Member, AIAA.

improvements in our understanding of the physical mechanisms involved. Direct simulations of transition [34] and the recently developed Parabolized Stability Equations [30, 31] have advanced theoretical-numerical work far ahead of the experimental database. Experimental work that describes not only the location of transition but also the mechanisms involved is needed in order to improve these modern theories.

Unambiguous progress in characterizing the mechanisms of low-speed transition has been made through the use of low-noise wind tunnels with disturbance levels comparable to those in flight, and the study of the development of controlled perturbations. In contrast, the interpretation of most high-speed experiments has been ambiguous due to:

1. Operation in high-noise wind tunnels with disturbance levels much larger than those in flight. The mechanisms of transition operational in small-disturbance environments can be changed or bypassed altogether in high-noise environments [48].

2. A lack of measurements carried out with controlled disturbances.

Slow progress overcoming the first difficulty has limited work on the second. Only in the last two decades have low-noise supersonic wind tunnels been developed [8, 68]. This development has been difficult, since the boundary layers on the nozzle walls must be kept laminar in order to avoid high levels of eddy-Mach-wave acoustic radiation from the normally-present turbulent boundary layers. The effects of this acoustic noise are profound. For example, linear instability theory suggests that the transition Reynolds number on a 5 degree half-angle cone should be 0.7 of that on a flat plate, but noisy tunnel data showed that the cone transition Reynolds number was actually higher than the flat plate result. Only when quiet tunnel results were obtained was the theory verified [17]. Consequently, both the location and the parametric trends for transition in conventional wind tunnels can be dramatically different from those in flight [48]. *Only the study of controlled disturbances in a controlled quiet environment can produce unambiguous data suitable for development of reliable theory.* Reliable predictive methods will have to be based on estimates of the flight disturbance environment.

The Purdue Quiet-Flow Ludwieg Tube

Quiet facilities require low levels of noise in the inviscid flow entering the nozzle through the throat, and laminar boundary layers on the nozzle walls. These features make the noise level in quiet facilities an order of magnitude lower than the 0.5 to 3 percent pressure fluctuations typical of conventional facilities. In order to reach these low noise levels, conventional blow-down facilities must be extensively modified. Requirements include a 1 micron particle filter, a highly polished nozzle with bleed slots for the contraction-wall boundary layer, and a large settling chamber with screens and sintered-mesh plates for noise-reduction [8]. To reach these low noise levels in an affordable way, the Purdue facility has been designed as a Ludwieg tube [54]. A Ludwieg tube is a long pipe with a converging-diverging nozzle on the end, from which flow exits into the nozzle, test section, and second throat (Figure 1).

A diaphragm is placed downstream of the test section. When the diaphragm bursts, a shock wave passes downstream, and an expansion wave travels upstream through the test section into the driver tube. The nominal end of the run occurs when the expansion wave has returned to the test section after reflecting from the upstream end of the driver tube. Since the flow remains quiet after the wave reflects, sufficient vacuum can extend the useful runtime to many cycles of expansion-wave reflection, during which the pressure drops quasi-statically.

Figure 2 shows the nozzle of the existing facility. The region of useful quiet flow lies between the characteristics marking the onset of uniform flow, and the characteristics marking the upstream boundary of acoustic radiation from the onset of turbulence in the nozzle-wall boundary layer. The usual quiet-flow length Reynolds number is based on the unit Reynolds number and the length on the centerline between the onset of uniform flow and the first arrival of noise radiated from the nozzle walls. **For an axisymmetric nozzle with a nominally uniform transition location, this quiet uniform-flow region will consist of back-to-back cones, each with a half-angle equal to the Mach angle. For many applications only the upstream-pointing cone will really be useful.**

Quiet-flow operation at length Reynolds numbers of about 400,000 has been demonstrated in the existing facility, making it suitable for measurements of receptivity and instability, but not complete transition to turbulence [54]. These quiet-flow results also show that the basic concept for the facility is sound. Recent work has shown that controlled perturbers and diagnostic instrumentation

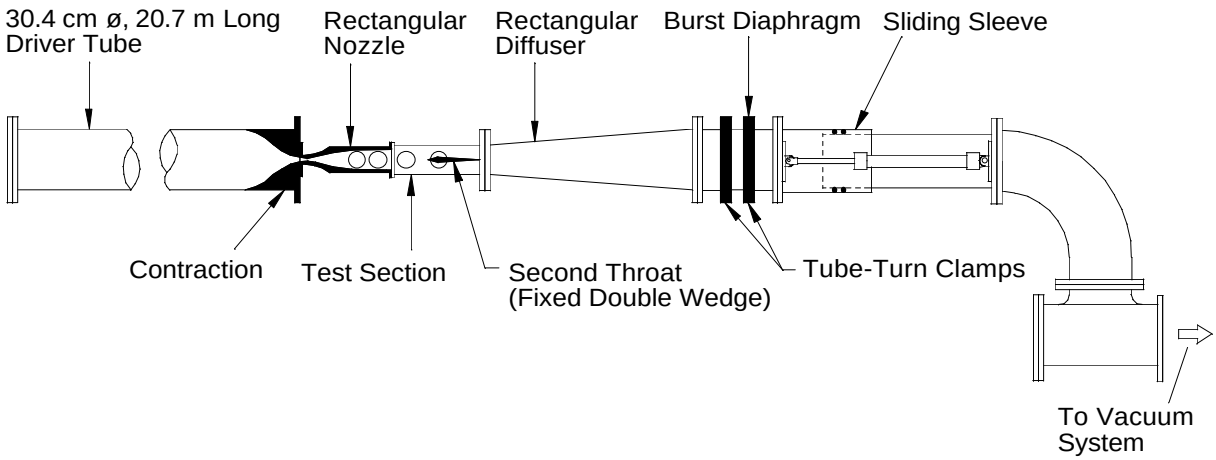

Figure 1: Schematic of Purdue Mach-4 Quiet-Flow Ludwieg Tube

can be developed and operated in the facility, and that useful instability measurements can be obtained [58, 53, 36, 37]. Operation with quiet flow at higher Reynolds numbers now requires only a larger and higher quality test section.

Conceptual Design

Need for a High Reynolds Number Quiet-Flow Hypersonic Wind Tunnel

In order to study the complete laminar-turbulent transition process under conditions comparable to flight, quiet-flow must be maintained to Reynolds numbers at which natural transition will occur on models of interest. What are the highest Reynolds numbers at which natural transition has been observed under low-noise conditions? Presumably, lower Reynolds-number transitions are then due to roughness, vibration, or some other effect.

High-Reynolds Number Transition in Symmetrical Flows

There are a number of cases in which very high Reynolds number transition has been demonstrated, apparently always in near-symmetrical flows. A sampling of these follows. Since the flight data is reviewed in reference [57], it will be summarized very briefly.

Re-Entry F: This flight test is documented in reference [70]. Re-entry of a 13-ft beryllium cone with a half-angle of 5 degrees and an initial nose radius of 0.1 inch was studied. The onset of transition was observed at values of Re_x based on freestream conditions that ranged from $19 - 22 \times 10^6$, at a freestream Mach number of about 20.

Sternberg V-2: A 8-ft long 10-degree half-angle cone was flight-tested at Mach 3 using a V-2 rocket [64]. The angle-of-attack was held to within 1 degree of 0.0, the wall was cold, and the nose radius was 'small'. Re_x at transition was clearly documented to reach 40×10^6.

Langley Mach-3.5 Quiet-Tunnel Cone/Plate: Both a round cone and a flat plate have been studied in the NASA Langley Mach-3.5 quiet-tunnel under low-noise conditions comparable to flight [17]. Measurements were made on an 18-inch flat plate, 11 inches from the leading edge. The bluntness was small and the wall was adiabatic. Transition onset was measured at $Re_x = 18 \times 10^6$. Measurements of the end of transition at $Re_x \simeq 24 - 27 \times 10^6$ have also been reported, although these seem to have been made somewhat outside the quiet-flow region [19]. Measurements on a sharp 5-degree half-angle cone were also made at zero angle-of-attack; Re_x for transition onset was reported at about 9×10^6, and the end of transition was reported to occur at about $12 - 14 \times 10^6$, although the end of transition was apparently not completely within the quiet-flow region. For these sharp-nose cases, the edge unit Reynolds number is nearly equal to the freestream unit Reynolds number.

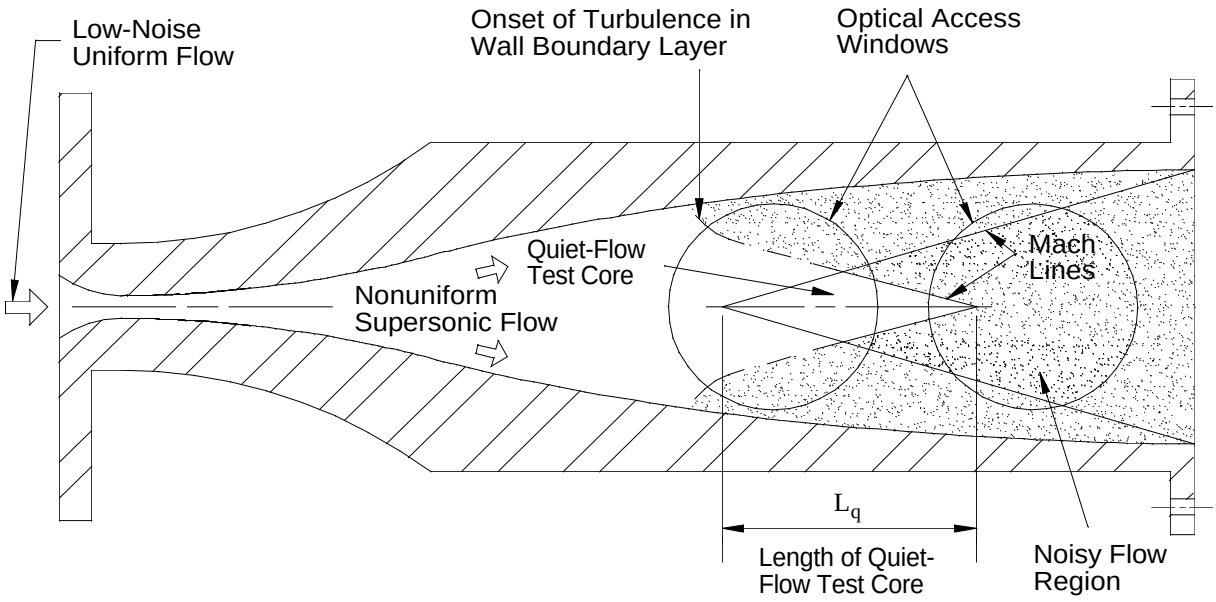

Figure 2: Schematic of Existing Mach-4 Quiet-Flow Nozzle

High Reynolds Number Transition in 3D Flows

Since geometries of practical interest will be maneuvering even when portions of the flow may be primarily symmetric, the 3D crossflow instability is likely to be important on all practical geometries. It is not expected to occur in the nearly-symmetrical cases described above. This class of flows seems to transition at consistently lower Reynolds numbers. The following cases are the ones with the highest transition Reynolds numbers that are known to the author. Of course, the length Reynolds number is clearly *not* the critical parameter for crossflow work; but length Reynolds numbers must still be discussed here to aid tunnel design.

Cattafesta Wing Leading Edge: A swept-wing leading edge model was tested in the Langley Mach 3.5 quiet tunnel [16]. The entire wing was not in the quiet-flow region, and the leading-edge sweep was 77 degrees. Transition onset was observed on most of the model under conditions where the length Reynolds number was about 5×10^6. Transition extent was not discussed. Both stationary and travelling crossflow waves seemed to be significant, the dominant mode apparently depending on the quality of the very high polish maintained near the leading edge.

Cone at AOA in Mach 3.5 Quiet Tunnel: A 5-degree half-angle round cone was tested at angle-of-attack in the Langley Mach 3.5 quiet tunnel [33]. The nose was sharp, the angle of attack (AOA) was varied between -4 and 4 degrees, and the entire cone was not always in the quiet-flow region. Transition onset was observed at length Reynolds numbers ranging from 8×10^6 (consistent with the above zero AOA data) to 2×10^6 (at the highest AOA). Transition extent seemed to be about 20% of the transition onset, but was not studied.

Space Shuttle Orbiter: Transition onset on the NASA Space Shuttle occurs during re-entry at Mach numbers ranging from 15 to 6 and at length Reynolds numbers ranging from 10×10^6 to 3×10^6 [12]. The primary cause for the variation is thought to be surface roughness. If a standard 0.75% scale model is tested at 40 degrees AOA under conditions similiar to those used in the Langley 20-inch Mach 6 tunnel (which is of the noisy conventional design), about 28×10^6 of quiet-flow length Reynolds number is needed to accomodate the entire model within the quiet-flow region. Note carefully that this requirement is for 28 million *to the maximum diameter*, or 56 million based on the end-to-end length of the quiet uniform region. Transition extent is a very significant factor in flight (it is normally given in seconds from re-entry), but data for the Reynolds-number ex-

tent have not yet been reduced, to the author's knowledge. Transition extent may depend on the wind-tunnel noise level, even for roughness-induced transition [48].

Summary of Reynolds-Number Requirements

The symmetric-flow data exhibits very high transition Reynolds numbers. However, transition on perfectly symmetric models is not very applicable to manuevering 3D vehicles. The first two of the asymmetric cases exhibit transition onset within an Re_x of 10×10^6. *Note that it is 10 million to the maximum diameter of the quiet region that is really required.* The downstream-facing part of the back-to-back cones that form the quiet uniform flow region is of little use, except for flat plates, and models with flat surfaces that can be placed along the tunnel axis. Since the Mach 6 flow may be more stable than the Mach 3.5 flow, it would be better if the flow was quiet to 20×10^6, again between the nose and maximum diameter of the quiet-flow region. Finally, to cover extent of transition and the Orbiter case, it would be even better if the flow was quiet to a length Reynolds number of 40×10^6, again up to the maximum diameter. **Since the only existing hypersonic quiet tunnel (the Langley Mach 6, which is now in a box) was only quiet to 3×10^6 to the maximum diameter [10], an order-of-magnitude improvement over the best existing technology is needed to fully meet estimated requirements.** However, a factor-of-4 improvement would be a substantial step, and would probably allow meeting the requirement for transition-onset measurements under 'natural' conditions. *The quiet tunnel is designed to stabilize the highly symmetric flow on an axisymmetric nozzle wall in order to delay nozzle-wall transition long enough to maintain quiet flow over an asymmetric model all the way to natural transition.*

Mach Number Issues

The second-mode instability, characteristic of hypersonic conditions, begins to become effective on cones and flat plates at Mach numbers between 5 and 6 [38]. Transition estimates based on e^N theory for a wall at 70% of the adiabatic wall temperature show that the second mode begins to dominate transition for a round cone at zero AOA at about Mach 5 [41, Fig. 9]. The second mode is clearly dominant under cold-wall conditions at Mach 6 [41, Fig. 10], although it takes until Mach 7 for it to dominate under adiabatic-wall conditions. The theoretical dominance of the second mode under cold-wall conditions at Mach 6 was confirmed by Stetson et al. [65]. Since most hypersonic vehicles are operated with wall cooling, and our facility has a short runtime, operation at a stagnation temperature of 350K and a model wall temperature of 245K appears to be a reasonable plan. The simplest operation will be with a stagnation temperature of 350K (just at the static liquefaction limit) and the model at room temperature (about 300K), where the second mode will probably still dominate the highly symmetrical zero-AOA cone flow.

Mach number affects not only this second mode. Reference [13] examines the effect of Mach number on the critical roughness Reynolds number Re_k, from data for 3 symmetric-flow cases in conventional wind tunnels. Figure 8 in that reference shows that the square root of the critical roughness Reynolds number jumps by a factor of 10 between Mach 4 and Mach 5. This is only a striking example of the well-known fact that it is very difficult to trip a hypersonic laminar boundary layer, presumably because most of the massflow is relatively far from the wall. Mach 6 will clearly be high enough to study many of these kinds of effects.

Although Mach 6 is in the low range of hypersonic conditions, the additional cost for reaching cold flow at Mach 8 is considerable, and in any case NASA Langley already has a major effort at Mach 8. It would be highly desirable to maintain quiet flow to hot hypersonic conditions, where dissociation and ionization occur, but the only paths that even seem possible are highly uncertain and expensive [24].

Summary of Design Methods

The methods used for design of the Ludwieg tube itself are taken from the standard literature on Ludwieg tubes [63, 15, 67]. The inviscid flow from the driver tube into the test section is readily described with standard isentropic flow equations [51, 47]. Details of the effect of the buildup of the boundary-layer on the wall of the driver tube, and how this changes the tunnel stagnation pressure, are treated in [51, 46]. The design of the second throat for the tunnel, the allowable model sizes, and the stagnation pressure losses in the diffuser are treated in detail by Pope and Goin [47], who also discuss the analysis of vacuum requirements. Minimum driver-tube temperatures for avoiding liquefaction are conservatively computed using the static liquefaction correlation [66].

The methods used for design of the quiet-flow

nozzles are very nearly the same ones used by NASA Langley for its designs. Reference [55] includes a detailed comparison showing that the author can repeat Frank Chen's computations of the N-factor for Görtler instability on the wall of the Langley Mach-6 quiet nozzle. The major difference from the Langley methods is that the supersonic uniform-flow-exit nozzle shape is computed using the wind-tunnel nozzle design code used for the AEDC tunnels [62], instead of a Chen-modified form of the short-rocket-nozzle code of Nelms. The Sivells code used already included the ability to create radial-flow sections between the initial expansion contour and the latter part of the contour (which cancels the characteristics in order to provide uniform flow at the exit). Harris's boundary-layer code is used for the laminar boundary-layer, just as by Langley [27]. Malik's e**Malik code is used for the e^N stability computations, as by Chen [39, 40]. The input/output of the three codes has been modified by the author, to create an automatic system that feeds the output of one code into the input of the next, with minimal user labor [55]. The bleed slot lip ahead of the throat is computed using the Hopkins-Hill technique, just as it has been at Langley, except a new, documented version was written [3]. The suction side of the bleed slot lip has been designed by the method of streamtubes, as was done by Beckwith [2]. The design of the contraction and bleed-slot area will be described together with the mechanical design in Reference [56].

Plan for Reaching High Quiet Reynolds Numbers

The baseline for the plan is the NASA Langley Mach-6 quiet nozzle, which was recently characterized and then decommissioned due to a space conflict [11]. The only other potential hypersonic quiet-flow nozzle is the Langley Mach-8 nozzle, which has been undergoing shakedown since early 1996 [68, 69, 4]. Considerable experience has been developed at NASA Langley, using various prototype nozzles primarily at Mach 3.5 and Mach 5. The following sections summarize the author's main conclusions from reviewing the many papers published by the Langley group.

Achievable Throat Finishes Limit Useful Stagnation Pressures

As the tunnel stagnation pressure is increased, the test-section unit Reynolds number increases. If the unit Reynolds number increases faster than transition moves upstream on the nozzle wall, then the quiet-flow length Reynolds number ($R_{\Delta x}$) will increase with pressure. Here, $R_{\Delta x}$ is based on the test-section unit Reynolds number and the axial length of uniform and quiet flow along the centerline. This is generally the case in the Langley data, up to some pressure p_m where $R_{\Delta x}$ reaches a maximum. The decreases in $R_{\Delta x}$ that occur beyond this pressure are thought to be caused by the increasingly strong effect of the roughness in the nozzle throat, for polishing the nozzle throat has a substantial effect on p_m, and therefore $R_{\Delta x}$. However, there is a limit to the polish achievable on the metals normally used. This is particularly true because it is the largest roughness element and not the average roughness which controls the effect of the roughness on transition. It would be very difficult to identify and remove all microscopic flaws from a large area of multiply-curved metal in a narrow inaccessible channel. The throat is the critical region because the boundary-layer is thinnest there; this theoretical expectation is confirmed by polishing experience.

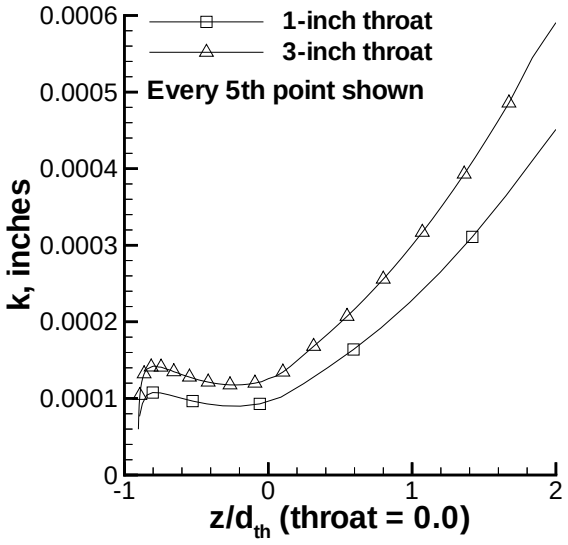

Figure 3: Allowable Peak Throat Roughness for Two Mach-6 Nozzles (a1,a2)

Figure 3 shows the allowable roughness height, k, computed in two Mach 6 nozzles at the same stagnation pressure, using the $Re_k = 12$ criteria suggested in many of the Langley papers. Here, z/d_{th} is the axial distance along the nozzle, normalized by the throat diameter. The characters in parentheses identify the two cases presented in the figure. The

two nozzles differ by a factor of 3 in size, and therefore the bleed-slot lip differs in length by a factor of 3, yet the allowable roughness height decreases only slightly with increasing bleed-slot length. Note that the throat boundary-layer is independent of the downstream Mach number, since all throats are at Mach 1. **It is likely that the stagnation pressure of the roughness-limited peak in quiet-flow Reynolds number depends mostly on the stagnation conditions and not on the test-section Mach number.**

To test this hypothesis, data has been collected from several Langley publications:

1. Reference [5] gives results for the Mach 3.5 2D pilot tunnel. Figure 5 therein shows $R_{\Delta x}$ reaching a maximum at a unit Reynolds number of about 1 million per inch. If the stagnation temperature was about 300K, this corresponds to about 100 psia, and a Reynolds number of $1.0 \times 10^8/m$ at the throat.

2. Reference [6] gives results for two polishes on the 2D Mach 3.5 nozzle and also for an axisymmetric Mach 3.5 nozzle. The axisymmetric nozzle and the best polish on the 2D nozzle both show $R_{\Delta x}$ reaching a maximum at about 40 million per meter, which is of course still about 100 psia at 300K. The lesser polish peaks at about 30 million per meter.

3. Reference [7] gives results for an axisymmetric Mach 5 nozzle. The peak in $R_{\Delta x}$ is here at about 10 million per meter. At the apparent stagnation temperature of about 400K, this is a stagnation pressure of about 80 psia, and a Reynolds number of $5.6 \times 10^7/m$ at the throat.

4. Reference [21] presents results for several Mach 3 and 3.5 nozzles of different lengths and polishes. The long axisymmetric Mach 3.5 nozzle gives values of $R_{\Delta x}$ about double those in the shorter Mach-3 axisymmetric nozzle. The shorter nozzle has an inflection-point wall angle of 15 degrees, while the longer nozzle has an inflection-point angle of 7 degrees, for about twice the length. The best polish on the long nozzle yields values of $R_{\Delta x}$ that peak at about 80 million/m, or about 200 psia, and a Reynolds number of $2.0 \times 10^8/m$ at the throat. The next-best polish still peaks at about 100 psia.

5. Finally, the initial polish on the Mach-6 nozzle showed good performance up to 233 psia (and probably about 450K, see p. 11 of [69]), and a Reynolds number of 1.4×10^8/m at the throat. However, later experience showed this was difficult to repeat, and the nozzle has seldom been operated above 150 psia.

Quiet-flow Reynolds number performance thus seems to be limited by roughness in the nozzle throat, above throat unit Reynolds numbers of about 1×10^8, or Mach-6 stagnation pressures of about 100-150 psia, unless extraordinary polishes are achieved (and these are difficult to maintain). Innovative technologies for achieving highly uniform throat finishes should be investigated (initially liquid coatings are one possibility for a breakthrough on this front). Since coatings with appropriate properties are not known to us, it seems that useful throat unit Reynolds numbers will be limited to about 1×10^8/m, or that useful Mach-6 stagnation pressures will be limited to 150 to 200 psia. Improvements in quiet-flow Reynolds number must be sought by increasing the length of the quiet-flow region. This path also has the advantage of increasing model size and model boundary-layer thickness, easing instrumentation requirements.

Lengthen the Nozzle to Achieve Higher Quiet-Flow Reynolds Numbers

Reference [21] shows experimental data to demonstrate that lengthening a nozzle extends the quiet-flow Reynolds number (see above). This concept is discussed in some detail with respect to another Langley Mach-2.4 design [18], which provides e^N computations. Figures 1 and 2 in [18] show that a 3X scale nozzle operated at 1/3 of the total pressure yields nearly identical quiet-flow length Reynolds number, with transition occurring in nearly the same relative location for the two nozzles. This indicates that Görtler-induced transition also scales with Reynolds number, as will be discussed further later. These figures also showed that a nozzle of approximately twice the length yielded quiet-flow length Reynolds numbers that are about double.

Heat the Nozzle Throat to Delay Transition

A further transition delay might be expected if the nozzle throat is heated [23]. Reference [42] explains the likely mechanism – note that although this second reference is for incompressible flow, the trend with wall cooling is the same for first-mode compressible waves, which may be a major factor in the first part of the nozzle. Although the effect of heating on the Görtler instability may be small, the heating will also thicken the throat-region boundary layer and so reduce the relative roughness height.

Langley observations indicate that a hot nozzle can increase the extent of quiet flow [28]. These results were confirmed indirectly by measurements in the Purdue tunnel carried out with hot driver-tube gas (to which the wall appears cold); these results show a decrease in quiet-flow Reynolds number [44].

Use Less Exotic Fabrication Processes and Build a Larger Nozzle

Standard Langley procedure specifies exotic wall-waviness tolerances of 0.0002 to 0.0005 inch/inch, in designs of axisymmetric quiet-flow nozzles (see, e.g., [68]). According to Ivan Beckwith, these arose from examination of two cases where larger tolerances caused problems with nonuniform mean flow [9, 25]. The two-dimensional Mach 3.5 quiet tunnel [9] had a waviness flaw of 0.002 inch/inch, which caused a Mach number variation of 0.045/inch on the centerline. This corresponds to a total pressure variation of about 4%, which was felt to be unacceptable, leading to a waviness specification of 0.0002 inch/inch, which would make the Mach number variation small. The Mach 3.5 data also showed that a nozzle-wall turbulent boundary layer interacting with the weak waves generated by the waviness increased the noise on the centerline [9, p. 4]. *It is important to note that there is no data suggesting that this waviness caused earlier transition of the nozzle-wall boundary layers.* Waviness *does* have an effect on transition when it is large enough [43]; the amount of waviness necessary to influence transition in a quiet-flow nozzle is not well understood.

In the axisymmetric case it is well known that any axisymmetric flaws in the nozzle contour create waves that focus on the centerline and therefore create relatively large variations in centerline Mach number. A joint in the original AEDC Tunnel B nozzle caused a Mach number variation from 8 to 7.9 to 8.1 and back to 8; this joint was caused by a maximum wall-waviness defect of about 0.003 inch/inch over 4.8 inches [25]. Figure 6b in [25] shows that the peak Mach number of 8.1 dropped to 8.0 about 1 inch from the centerline of the 48-inch diameter of the nozzle. The nozzle was remachined to reduce the peak by a factor of 3 or so, to a Mach number variation of 0.01 per inch, with a nozzle waviness of 0.0004 inch per inch.

There is a limited amount of data to show that noise may also focus on the centerline [52], and at least one study has been carried out of the effect of axial location on transition in the Langley Mach 3.5 quiet tunnel [20]. However, the author is unaware of any detailed study of the interrelation of noise, contour accuracy, and mean flow accuracy in axisymmetric nozzles.

The waviness specifications used by NASA Langley have consistently pushed the state-of-the-art for fabrication processes, and therefore resulted in very high costs. Although high mean-flow uniformity is desirable, there is no evidence that it is crucial to the maintenance of quiet flow. Mean flow variations that are only significant very near the centerline will in any case either be ahead of the model, in which case they may have no effect, or inside the model, in which case the model will see an axisymmetric mean disturbance of small amplitude. The author believes that these flaws can be managed with suitable model positioning – the model can be moved upstream and downstream, or off the centerline, and the effect studied. A wall-waviness specification of 0.001 or 0.002 inch/inch can be reliably achieved with a good NC lathe, and also reliably measured. Such a specification makes the nozzles cost 2 to 4 times less than nozzles fabricated to a 0.0005 or 0.001 inch/inch specification; the author believes that the funding is better used to more directly increase the length of quiet flow.

Steps in the nozzle-wall contour at joints between sections are of greater concern, especially upstream, where the Mach number is lower and the boundary layer thinner. These steps can be minimized by good shop practice; whether the remaining flaws are significant or not will be proven by tests of the new Langley Mach-8 nozzle and of the proposed prototype Mach 6 nozzle.

Build a 9-inch Prototype for the 24-inch Nozzle

The prototype will address the following technical risks:

1. Is transition affected by the nozzle joints?
2. Can we time the bleed-slot suction successfully? This suction must not start too long before acceleration of the main flow, or the contraction-region gas will be disturbed before it flows into the test section. Neither can it start too long after main flow begins, or too much of the run will be noisy due to early transition of the boundary-layer that has spilled around the bleed-slot lip. A passive delay system is planned.
3. Custom aspheric windows are proposed to match the nozzle walls and provide optical ac-

cess to the first part of the uniform quiet-flow region. Do these work OK?

4. Can heating of the bleed slot improve the quiet-flow Reynolds number?

5. How much does the nozzle end up costing? How much do the waviness specifications accepted cause problems in Mach-wave focusing of flaws into centerline mean-flow deviations? Are these a significant problem for the experimental work?

6. The driver-tube will necessarily operate at higher Reynolds numbers. Although the driver-tube boundary layer may be laminar now, it will almost certainly be turbulent then. Will this cause significant noise increases?

7. Does a longer nozzle really allow for more quiet flow, even at Mach 6?

Massflow for the 9-inch Mach-6 Prototype

The current Mach 4 nozzle has a massflow of 0.5 pounds/sec at 1 atm. total pressure, or about 5 pounds/sec at 10 atm. The driver-tube Mach number is 0.0066, to maintain a high contraction ratio and a small pressure drop during the extended run made possible by the large vacuum. During a 0.9s run, about 12% of the driver-tube mass flows out, ensuring a slow rate of pressure decay; it is thus possible to do quasi-steady testing at a variety of Reynolds numbers during a single run, which has proven to be most useful [59]. A 9.4-inch diameter Mach-6 nozzle has slightly less massflow, about 3.2 pounds/sec at 130 psia. The mass that flows out of a 12-inch driver tube during the 0.9 s run is still about 12% of the initial driver-tube mass. The massflow from the new 18-inch stainless-steel driver tube will be less. The energy release rate will be about 100 kW. About 3 times as much vacuum is required for Mach-6 operation, primarily because a larger pressure drop must be maintained at the higher Mach number. The runtime would thus be expected to drop to about 1 second from the current 3.5 seconds; however, a surplus 3800 cubic foot vacuum tank will be used in place of the current 500 cubic foot tank, allowing a 7-second run. The thrust is about 120 pounds.

Massflow for the 24-inch Mach-6 Ludwieg Tube

This nozzle would require a new Ludweig tube with a 24 or 30-inch driver tube that is 200-ft long. A 24-inch driver tube is sufficient to drive a 24-inch Mach-6 test section, and still have about 10% massflow during a 1 sec. run. The driver-tube Mach number is a low 0.014, comparable to that in the existing facility. The 30-inch driver could be pumped to 10 atm. with our existing 50-hp 200-scfm compressor in about 50 minutes, maintaining about 1 hour between runs. A vacuum pump of about 25 hp would be needed to pump down the 3800 cubic-foot surplus vacuum tank in about an hour. With a 130 psia charge pressure, the massflow in the 24-inch Mach-6 test section would be about 30 pounds/sec, with a thrust of about 1000 pounds and an energy release rate of about 1 megawatt during the run.

e^N Results

Nozzle Shapes

Figure 4 shows the inviscid contours of three nozzles designed with Sivell's code [61]. A 3rd-degree axial velocity distribution was chosen in the throat region, and a 4th-degree velocity distribution was chosen in the exit region. The contour of the Langley Mach-6 quiet tunnel is also shown – this contour includes the displacement thickness correction. Some key parameters are shown in Table 1. Here, ID is the case number for the nozzle; each nozzle was assigned a letter identifying the inviscid design, followed by a number identifying the viscous conditions. These ID's will be shown in parentheses in the plots. Also, η is the wall angle at the inflection point in degrees, RC is the radius of curvature at the throat, x_g and y_g are the axial and radial locations of the beginning of radial flow at the wall, x_a and y_a are the axial and radial locations of the end of radial flow at the wall, and x_d and y_d are the exit of the nozzle at the wall. All lengths are given in throat radii, and the coordinate origin is on the centerline at the throat. The nozzles were scaled geometrically to various sizes. Nozzle `m6chen6` is very similar to the Langley Mach-6 design, although the similarity is obscured somewhat in this plot since the Langley exit diameter is 7.5 inches. The long nozzle, `g`, has half the inflection-point angle and about twice the length. The very long nozzle, `l`, has an inflection angle which is halved again. The 4th nozzle, `m`, was shortened because the additional length is not needed for the prototype. The 5th nozzle, `l`, is the same as `i`, except it was computed with higher resolution. The length of the radial flow region generally increases with nozzle length.

ID	η	RC	x_g	y_g	x_a	y_a	x_d	y_d
m6chen6	9.84	3.68	3.39	1.50	12.82	3.13	81.85	7.29
mach6g	4.92	4.00	1.81	1.13	28.42	3.42	142.1	7.29
mach6i	2.46	8.00	1.43	1.05	72.32	4.09	240.7	7.29
mach6m	4.00	8.00	2.13	1.12	38.31	3.65	164.9	7.29
mach6l	2.46	8.00	1.43	1.05	72.32	4.09	240.7	7.29

Table 1: Key Parameters for Inviscid Nozzle Designs

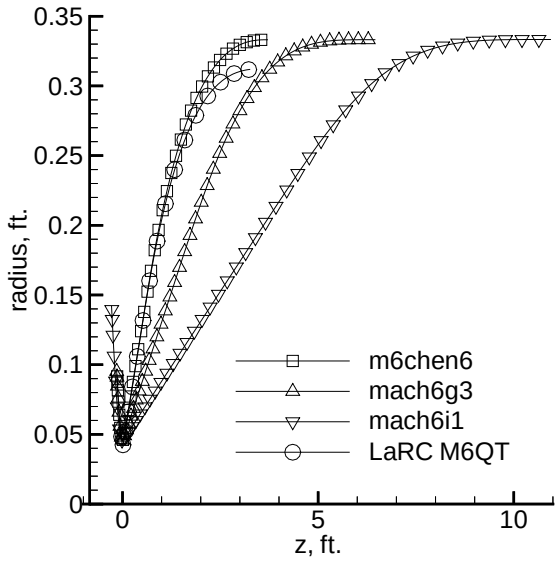

Figure 4: Inviscid Contours for 3 Axisymmetric Nozzles with 8-inch exits

Further Validation

Figure 5 shows computations for the nozzle similar to that used at NASA Langley, with an adiabatic wall. Envelopes of the 1st-mode and Görtler computations are shown, for two stagnation pressures. The results are similar to those reported (in lesser detail) by Chen; Görtler instability dominates. Here, the nozzle wall is adiabatic, $T_t = 820$R, the stagnation pressure is shown in the legend, and the inviscid exit diameter (without the displacement thickness correction) is 8.0 inches. Several individual frequencies are computed for each case, but only the envelope of the most amplified frequency at each station is plotted here. The automated system requires little user intervention. About 20-40 hours cpu time is required to complete each computation; most of this for the 1st mode. The speed of the 167 MHz Sun Ultrasparc 1 cpu used for the computations is quoted as 6.39 for SPECint95 and 11.80 for SPECfp95. Since this is roughly twice as fast as a 200mHz Pentium Pro, these computations were not very expensive. However, a job had to be kept in the queue evenings and weekends for 6 months in order to complete them all, since it took about a week to accumulate 40 cpu hours on our department server.

Figure 6 shows the quiet-flow length Reynolds number for the shorter nozzles, computed and compared to results for the Langley Mach 6. The Langley data was digitized from Figure 9 in Reference [22]. The TS and Görtler N-factors were combined by taking the square root of the sum of the squares, a procedure similar to that used successfully by Schrauf for crossflow and TS instability on swept wings [60]. Of course, there are many uncertainties in a semi-empirical prediction method of this type; these uncertainties include nonlinear effects in the growth of individual instabilities, nonlinear effects in the combined effects of several instabilities, and receptivity effects. PSE computations would have been useful but were not considered cost-effective.

Earlier predictions by Chen [22] agreed well with data in the Langley quiet nozzles when an N-factor of 7.5 was used as a transition criterion. Chen used

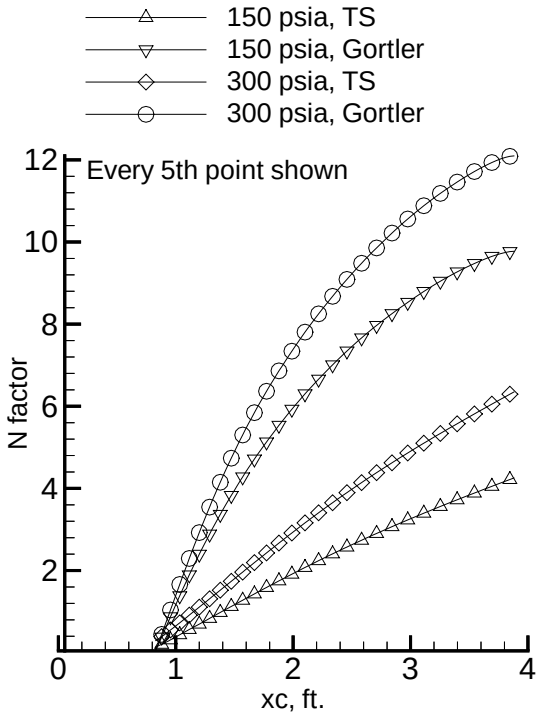

Figure 5: Envelopes of TS and Görtler Instability for a Short Nozzle at Two Reynolds Numbers (m6chen6b,m6chen6c)

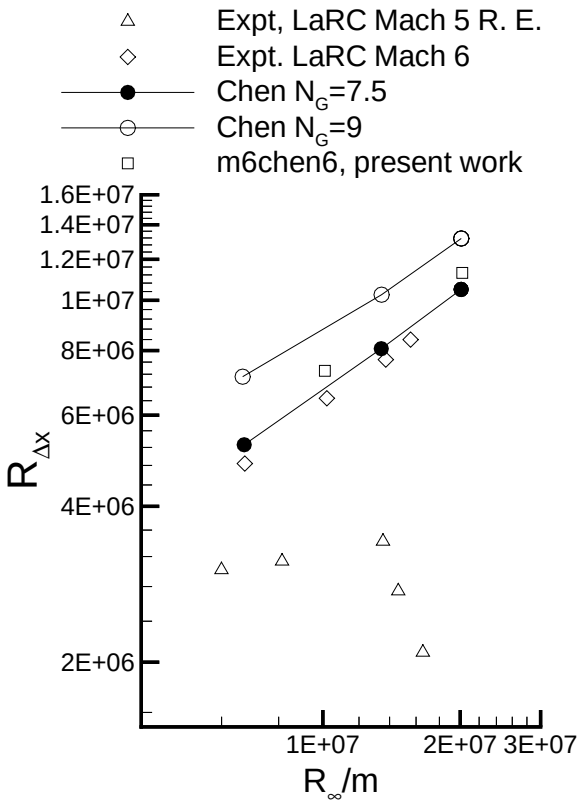

Figure 6: Quiet Reynolds Numbers for Chen and Chen-like Nozzles (m6chen6b,m6chen6c)

$N = 7.5$ based on *only the most amplified instability*; the 2nd-mode instability was not computed, and since the N-factor for the first mode was 2 or 3 it was neglected also (private communication). Here, transition will be based on the 'combined N-factor', N_{tot}, which is the square root of the sum of the squares of the individual N factors. Predictions will be based primarily on $N_{tot} = 7.5$, which is more conservative than Chen's method since it includes the effect of the smaller instabilities.

Using this method, transition was predicted on the nozzle walls, and the characteristic lines from the inviscid nozzle solution were used to predict the extent of quiet flow. The results for N=7.5 are very similar to Chen's results, and to the original data from the Mach 6 quiet tunnel. The new nozzle performs a bit better, for the results are similar even though the TS N-factor is included in our prediction method. The slope is about the same; the quiet Reynolds number increases with nozzle Reynolds number.

Scaling

Figure 7 shows results computed in the long nozzle at the same nozzle Reynolds number, to determine Reynolds number effects. The two cases achieve Reynolds number by a different combination of size and pressure. When scaled with Reynolds number and exit diameter, the results for the momentum thickness and Görtler number are identical. Görtler number G is defined as $G = (U\theta/\nu)\sqrt{\theta/R}$, where U is the edge velocity, θ is the momentum thickness, ν is the kinematic viscosity at the boundary layer edge, and R is the concave-wall radius of curvature. Görtler number thus scales with size and Reynolds number. The stagnation temperature is 820R, and the stagnation pressure and nozzle exit diameter are shown in the legend. The nozzle wall is isothermal for these computations, with an inlet temperature equal to the stagnation temperature, 820R, and a wall temperature that tapers linearly to 540R. This is similar to the temperature expected to develop normally in the tunnel – the driver tube must be continuously maintained at stagnation temperature for Mach 6, and it will heat the upstream end of the nozzle by conduction. The downstream end will be cold due to conduction to the piping and vacuum tank.

Figure 8 shows N-factor results for the same two cases. The envelope of the most amplified 1st-mode and Görtler waves is plotted, for each nozzle. The horizontal axis is the arclength along the nozzle wall scaled with the nozzle exit diameter. The curves overlap to within 1 percent. Thus, the instability computations scale with diameter and Reynolds number, even though the frequencies and Görtler wavenumber differ by a factor of 2. Reynolds number can be achieved with size or pressure, and the e^N results are identical in either case. This plot serves to validate the computational methods as well as the scaling.

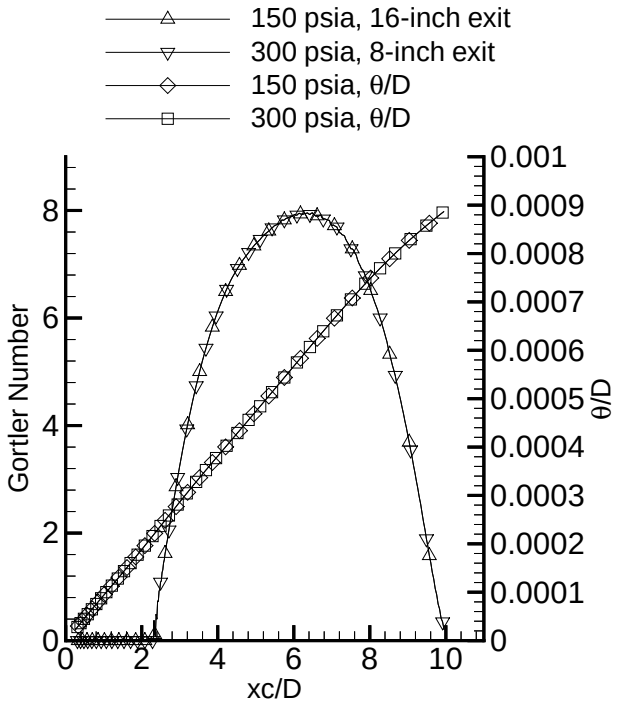

Figure 7: Görtler Number for Two Long Mach-6 Nozzles with Different Scalings (g5,g6)

Effect of Reynolds Number

Figure 9 compares N-factors in the long Mach 6 nozzle, at three Reynolds numbers. For all the cases, the stagnation pressure, P_t, is 150 psia, the stagnation temperature, T_t, is 820R, and the wall temperature is isothermal, decreasing linearly with arclength from 820R at the bleed lip to 540R at the exit. The exit diameters are shown in the legend. Both TS (1st mode) and Görtler rise with Reynolds number.

The 2nd-mode computations for these 3 cases are shown in Figure 10. The number of frequencies computed were insufficient to give smooth curves,

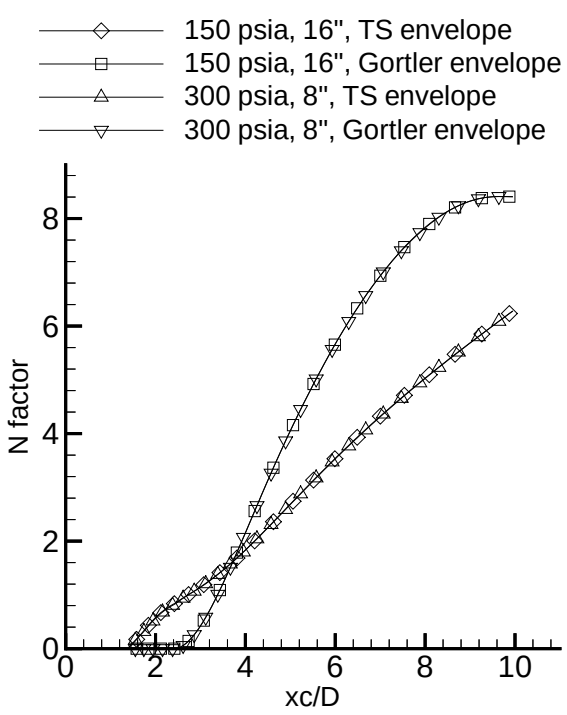

Figure 8: TS and Görtler Envelopes for Two Nozzles at Different Scales but the Same Reynolds Number (g5,g6)

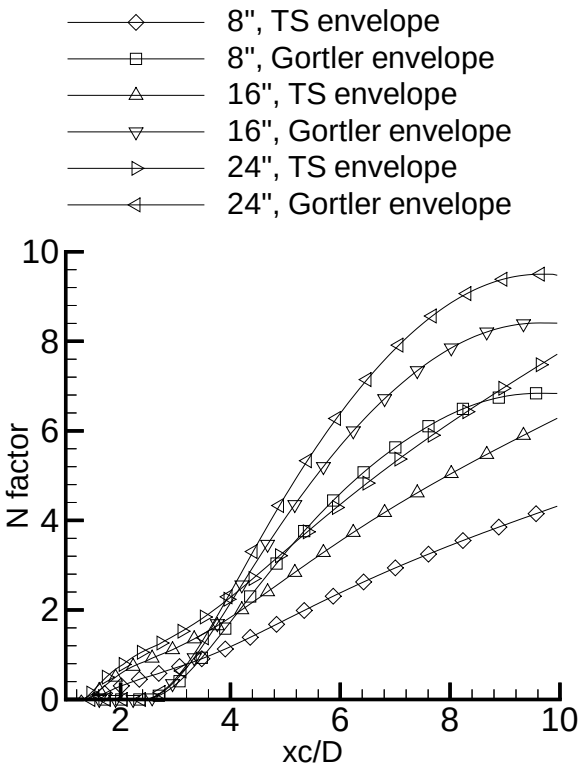

Figure 9: N-factor Envelopes at Three Reynolds Numbers (g3,g5,g4)

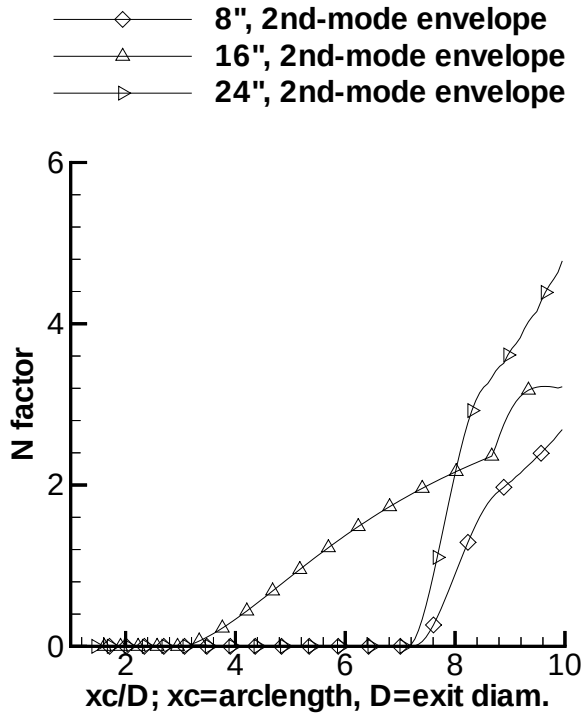

Figure 10: 2nd-Mode N-factor Envelopes at Three Reynolds Numbers (g3,g5,g4)

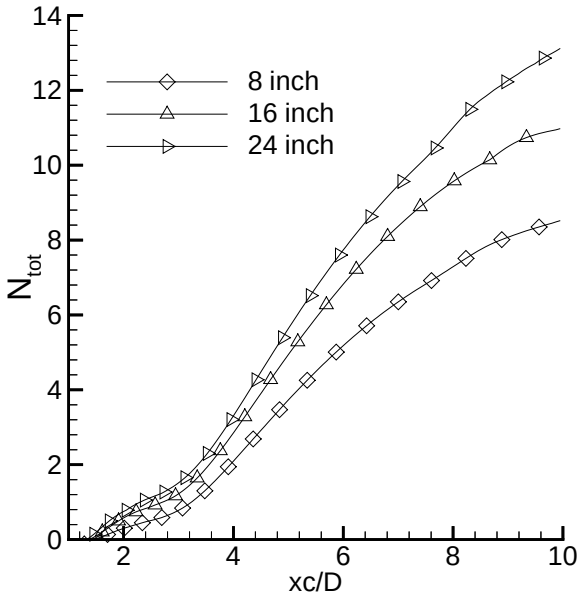

Figure 11: Total N-factors at Three Reynolds Numbers (g3,g5,g4)

but the increase in 2nd-mode growth with Reynolds number can still be seen.

Figure 11 shows the envelope of the three N-factors, again taken with the square root of the sum of the squares. Using N=7.5 the quiet Reynolds number was computed, with the results given in Table 2. Here, xc is the arclength along the nozzle wall from the bleed lip tip, D_q is the diameter of the quiet uniform region, and L_q is the length of the quiet uniform region, from tip to tip. The quiet Reynolds number increases with Reynolds number, but not as fast as it did for Chen's shorter nozzles. The performance of the long 8-inch is about 50% better than the Langley 7.5-inch Mach 6; the performance of the 24-inch is about 2 times better.

Effect of Nozzle Length
at Moderate Reynolds Number

Figure 12 shows the shape and curvature of the very long nozzle, with an 8-inch inviscid exit diameter. The radius of curvature is smooth, although some wobbles remain near 7 ft. These cause small wobbles in the Görtler N factors.

Figure 13 shows momentum thickness and

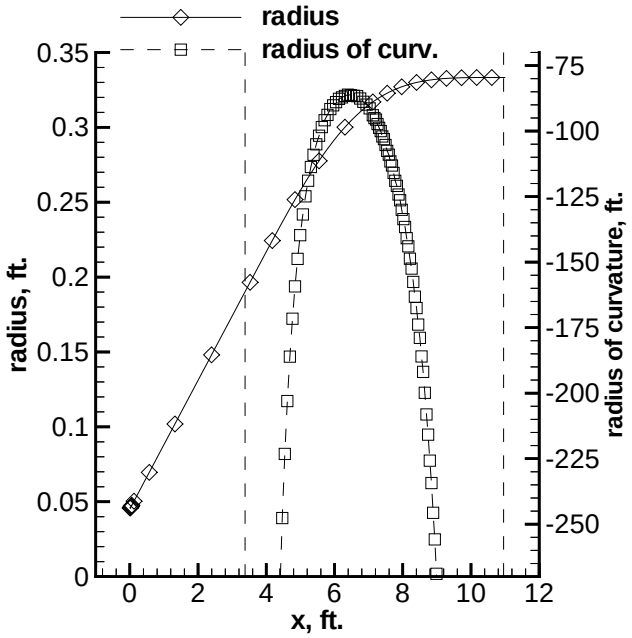

Figure 12: Contour and Curvature of Very Long Nozzle (i1)

ID	exit diam.	$N = 6.5$	$N = 7.5$	Re_{quiet}	D_q	L_q
g3	8 inch	$xc = 4.80$ ft.	$xc = 5.49$ ft.	8.7 million	0.48 ft.	2.8 ft.
g5	16 inch	$xc = 7.83$ ft.	$xc = 8.57$ ft.	9.7 million	0.53 ft.	3.2 ft.
g4	24 inch	$xc = 10.8$ ft.	$xc = 11.9$ ft.	11.4 million	0.62 ft.	3.7 ft.

Table 2: Quiet Reynolds Number vs. Reynolds Number for Long Nozzle

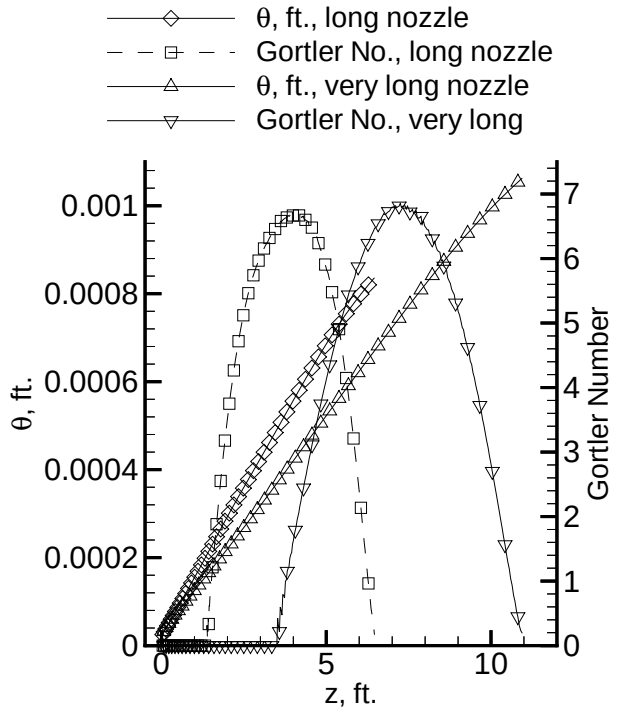

Figure 13: Momentum Thickness and Görtler Number in Long and Very Long Nozzles (g3,i1)

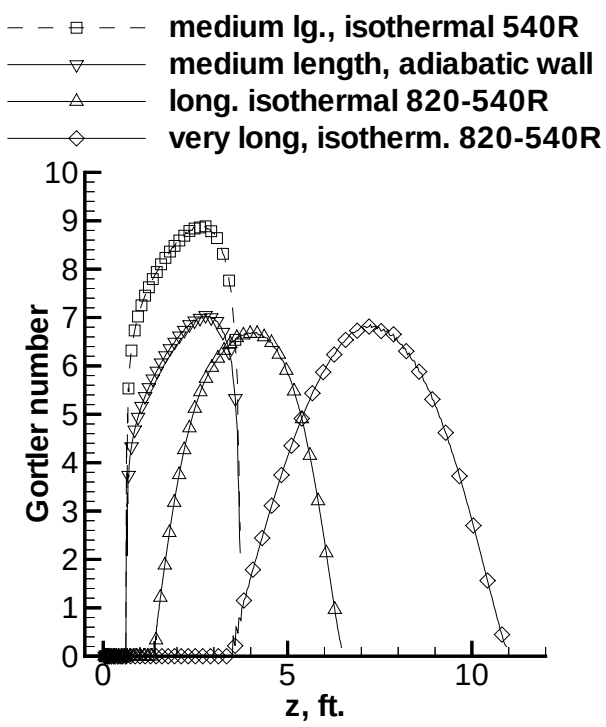

Figure 14: Görtler Numbers in Three Nozzles of Different Length (m6chen6,m6chen6b,g3,i1)

Görtler number for the long and very long nozzles. As is true in general unless otherwise stated, both computations were carried out at $P_t = 150$ psi and $T_t = 820$R. Both nozzles also have isothermal wall temperatures that decrease linearly with arclength from 820R at the bleed lip tip to 540R at the exit, and both have 8-inch exit diameters. Görtler number remains about the same as the nozzle is lengthened.

Figure 14 shows Görtler number for 4 nozzles detailed earlier. Only the wall temperature condition appears to have a marked effect.

Figure 15 shows 1st-mode and Görtler envelopes for three 8-inch nozzles, all at $P_t = 150$ psia and $T_t = 820$ R. As stated earlier, `m6chen6b` has an adiabatic wall, while `g3` and `i1` have isothermal

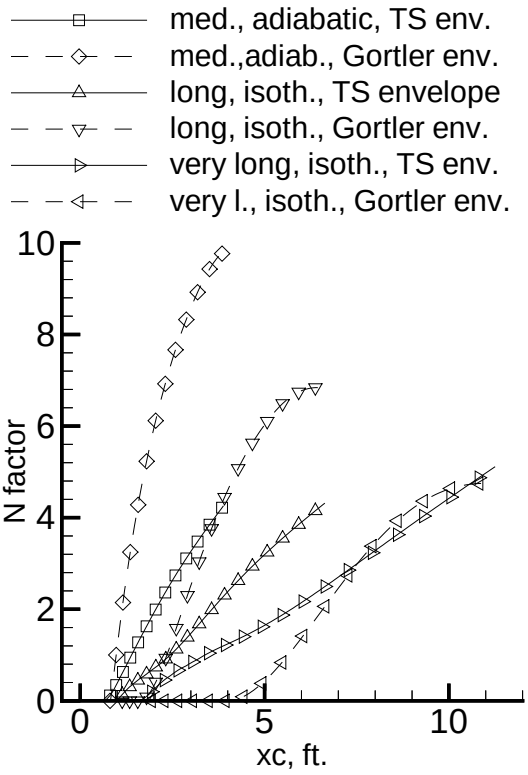

Figure 15: N-factor Envelopes for Three Nozzle Lengths (m6chen6b,g3,i1)

walls with a temperature that drops linearly with arclength from 820R to 540R. The Görtler N-factors drop dramatically when the nozzle is lengthened, but the 1st-mode increases with length for the two isothermal wall cases. *Although peak Görtler number does not decrease when the nozzle is lengthened, Görtler N factors do decrease. The use of transition estimates based on the N-factors rather than the Görtler numbers is supported by previous Langley experience with lengthened nozzles [21].*

Figure 16 shows the combined N-factors for the 3 nozzles, along with the 2nd-mode envelopes. The long and very long nozzles have the same temperature distribution, the medium nozzle is similar to the Langley design and has the adiabatic wall temperature used at Langley. The key quiet-flow parameters are summarized in Table 3. The quiet Reynolds numbers increase with length because the 1st-mode instability increases less than the Görtler instability decreases.

Effect of Length at High Reynolds Number

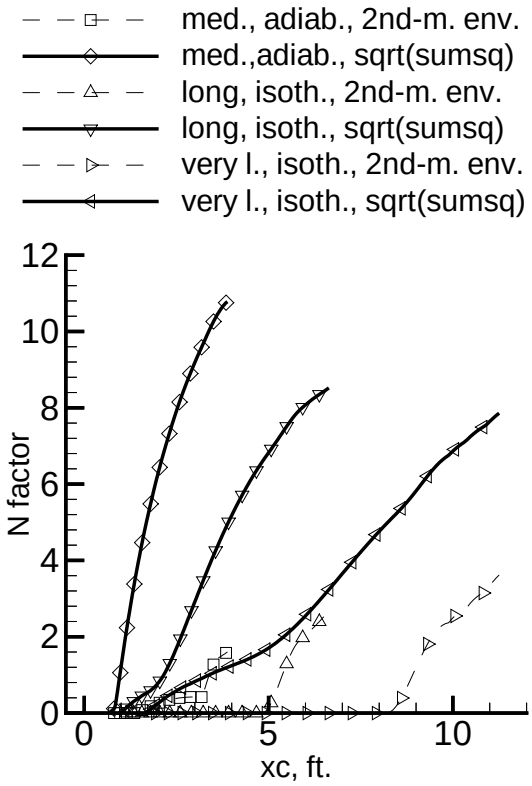

Figure 16: Total N-factors for Three Nozzles of Different Length (m6chen6b,g3,i1)

ID	$N = 6.5$	$N = 7.5$	Re_{quiet}	D_q	L_q
m6chen6b	$xc = 2.07$ ft.	$xc = 2.37$ ft.	7.3 million	0.40 ft.	2.4 ft.
g3	$xc = 4.80$ ft.	$xc = 5.49$ ft.	8.7 million	0.48 ft.	2.8 ft.
i1	$xc = 9.64$ ft.	$xc = 10.90$ft	11.1 million	0.61 ft.	3.6 ft.

Table 3: Quiet Reynolds Number vs. Nozzle Length

Figure 17 shows the results for the very long nozzle when it is scaled up to increase the Reynolds number by a factor of 3. It is compared to the long nozzle at the same Reynolds number. Both nozzles now have 24-inch inviscid exit diameters. The computations are again at $P_t = 150$ psia and $T_t = 820$R, and both nozzles have wall temperatures that taper linearly from 820R to 540R. Every 10th point is shown. Using $N_{tot} = 7.5$ as a transition criterion, the very long nozzle has a quiet Reynolds number of 7.8 million, while the long nozzle has a quiet Reynolds number of 11.4 million.

The very long nozzle in the 24" exit size has *worse* performance than it does in the 8-inch exit size. It also has worse performance than the long 24-inch nozzle does (although the very long 8-inch is better than the long 8-inch). TS dominates the very long nozzle, whereas it is less than Görtler in the long nozzle. The combined N-factor is also shown. Although N_{tot} is lower at the nozzle exit for the very long nozzle, its performance is worse because N=7.5 is reached farther upstream of the nozzle exit. This is shown in detail in Figure 18, which shows the nozzle shapes. The characteristics marking the onset of uniform flow are also shown, along with the characteristics marking the onset of noise radiated from the predicted transition location. There is less quiet uniform flow in the very long nozzle.

Although lengthening the nozzle works well at the lower Reynolds number, the improvement is not sustained at higher Reynolds number due to increased problems with the 1st-mode instability. Another means of control is needed in order to reach high quiet Reynolds numbers.

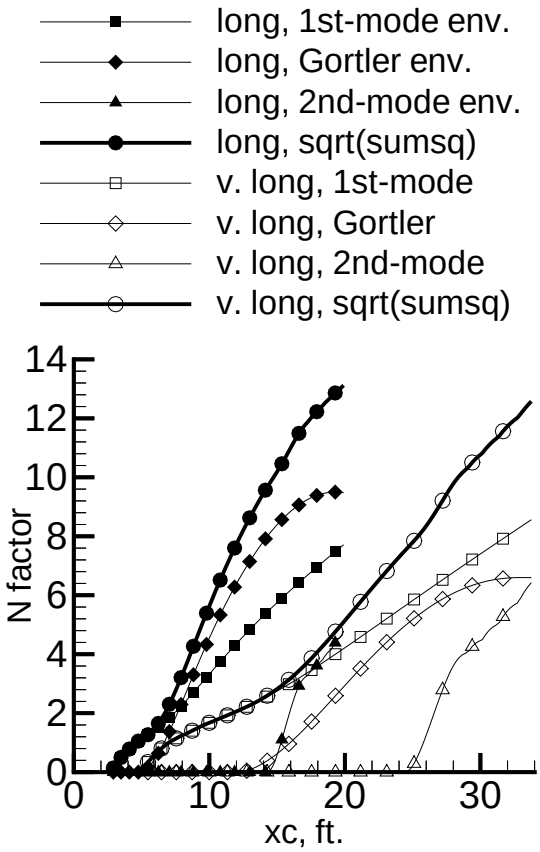

Figure 17: N-factors for Long and Very Long Nozzles at Higher Reynolds Number (g4,i2)

Effect of Nozzle Wall Temperature

It has already been shown that the temperature distribution at the nozzle wall is very important. A number of cases were then computed in order to see if the combined effect of wall temperature and nozzle length would allow reaching high quiet Reynolds numbers.

Figure 19 shows the temperature distributions for 4 such cases. All the nozzles have 24-inch inviscid exit diameters, and are computed at $P_t = 150$

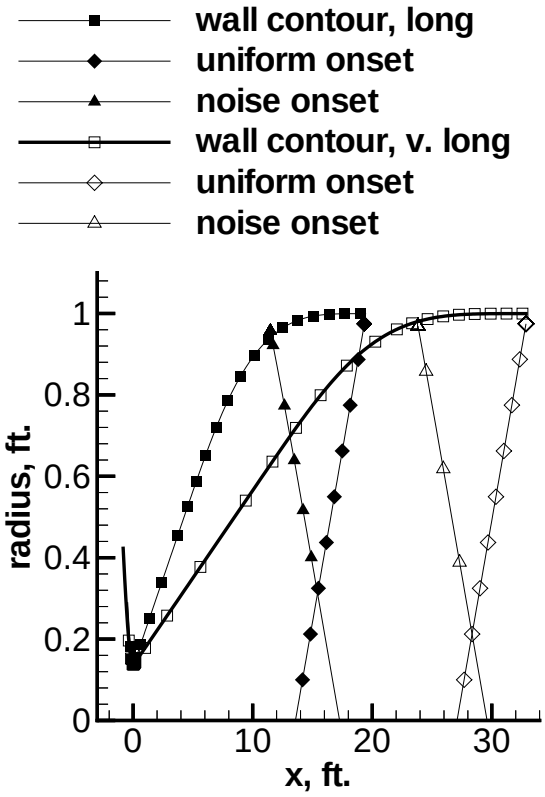

Figure 18: Quiet-Flow Boundaries in 2 Axisymmetric Nozzles with 24-inch exits (g4,i2)

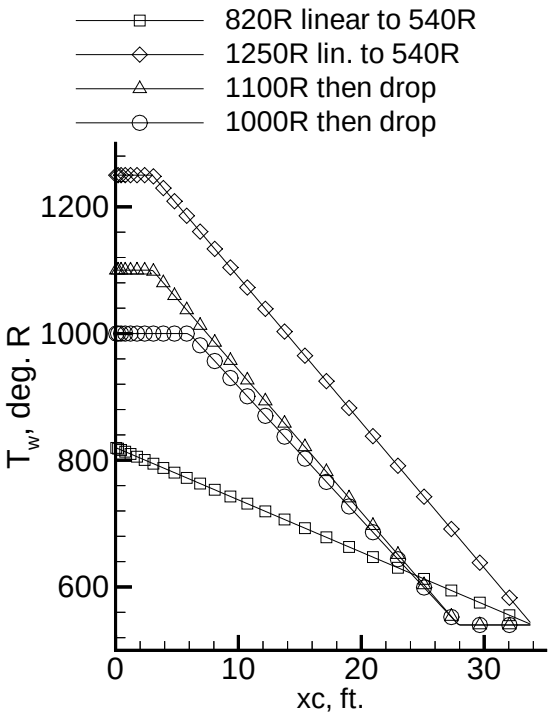

Figure 19: Various Wall Temperature Distributions for Very Long Nozzle (i2,i3,i4,i5)

psia and $T_t = 820$ R. The first case, `i2`, begins with a wall temperature equal to the stagnation temperature, 820R. It tapers linearly to nominal ambient temperature, 540R, at the nozzle exit. This simulates a throat maintained at the driver-tube temperature of 820R, and a nozzle exit cooled to maintain it at 540R, with a nominal constant-thermal-resistance path in between. The second case, `i3`, shows a throat maintained at 1250R over the first 3 feet of arc length, followed by the same linear gradient down to ambient temperature at the exit. The third case, `i4`, is similar, except the throat is heated only to 1100R, and the last 6 feet of the nozzle is held at room temperature. This simulates a case where the heat is taken out of the nozzle upstream of the last section where the windows are. The final case, `i5`, reduces the peak throat temperature further to 1000R, but spreads it over a longer distance, 6 feet, easing thermal-stress issues while maintaining a similar amount of total heat transfer into the boundary layer.

Figure 20 shows the dramatic effect of substantial heating at the throat. The envelopes of the most unstable waves are plotted for each nozzle, for each

of the 3 types of instabilities, and for the square root of the sum of the squares. The Görtler instability is affected only weakly by the heating. The 1st-mode instability decreases dramatically, causing a dramatic decrease in the summary N-factor.

Only the throat is heated, so the 2nd-mode instability, which grows only near the exit, should not be affected much. Uniform heating decreases the growth of the 2nd mode, so a decreasing wall temperature should make the wall look cold, increasing the 2nd-mode growth. Unexpectedly, however, the 2nd-mode waves decrease with the throat heating. This effect remains to be explained.

Throat heating is thus a very effective means of controlling the 1st-mode waves, and it also has a favorable effect on the 2nd-mode waves. Table 4 summarizes the key results. For case `i3` with the 1250R throat, N_{tot} doesn't reach 7.5 before the exit, where the computation halted. Transition is assumed at the nozzle exit, for a quiet Reynolds number in excess of 35.6 million. Quiet flow is predicted for a back-to-back cone with a half-length of 5.7 feet and a diameter of 1.9 feet. *Lengthening the nozzle controls Görtler instabilities, but causes problems with TS instabilities. However, when a long nozzle and a hot throat are combined, the result is a dramatic improvement.*

Figure 21 shows the effects of two lesser throat heating conditions, which are also summarized in Table 4. The case with the hotter throat shows less 1st-mode growth; this lesser growth makes a bigger different in transition location when $N = 7.5$ places transition near the exit, where N grows rapidly.

Further Validation Near Design Point

Since the performance of the very long heated-throat nozzle is unprecedented, further validation was performed near this design point.

Figure 22 shows two representations of the very long nozzle, both with an 8-inch exit diameter. Case `l1` has 399 points downstream of the throat, while the earlier case `i1` has 255. Every 20th point is shown. This set of studies was carried out to check the effect of grid resolution on the results.

Figure 23 shows the results for the 1st-mode waves in the throat of the fine-grid nozzle. The throat is heated to 1250R over the first 3 feet; the isothermal wall temperature then decreases linearly to 540R at the nozzle exit. The total pressure is 150 psia and the total temperature is 820R. The first mode grows rapidly in the heated throat, and is then damped downstream. The wave angles vary from 75 to 46 degrees. The data for this plot took

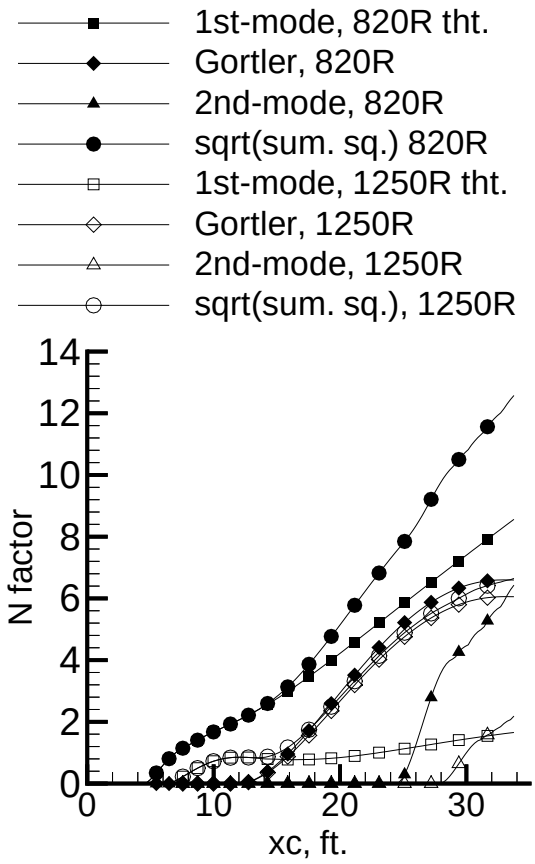

Figure 20: Effect of Additional Throat Heating in Very Long Nozzle (i2,i3)

ID	$N = 6.5$	$N = 7.5$	Re_{quiet}	D_q	L_q
i2	$xc = 22.5$ ft.	$xc = 24.4$ ft.	7.8 million	0.42 ft.	2.5 ft.
i3	$xc = 32.4$ ft.	past exit	35.6 million	1.95 ft.	11.5 ft.
i4	$xc = 29.9$ ft.	past exit	35.6 million	1.95 ft.	11.5 ft.
i5	$xc = 28.7$ ft.	$xc = 31.9$ ft.	30.6 million	1.67 ft.	9.9 ft.
l2	$xc = 32.5$ ft.	past exit	35.6 million	1.95 ft.	11.5 ft.
l3	$xc = 28.4$ ft.	$xc = 31.0$ ft.	28.0 million	1.53 ft.	9.1 ft.

Table 4: Quiet Reynolds Number vs. Wall Temperature for the Very Long 24-inch Nozzle

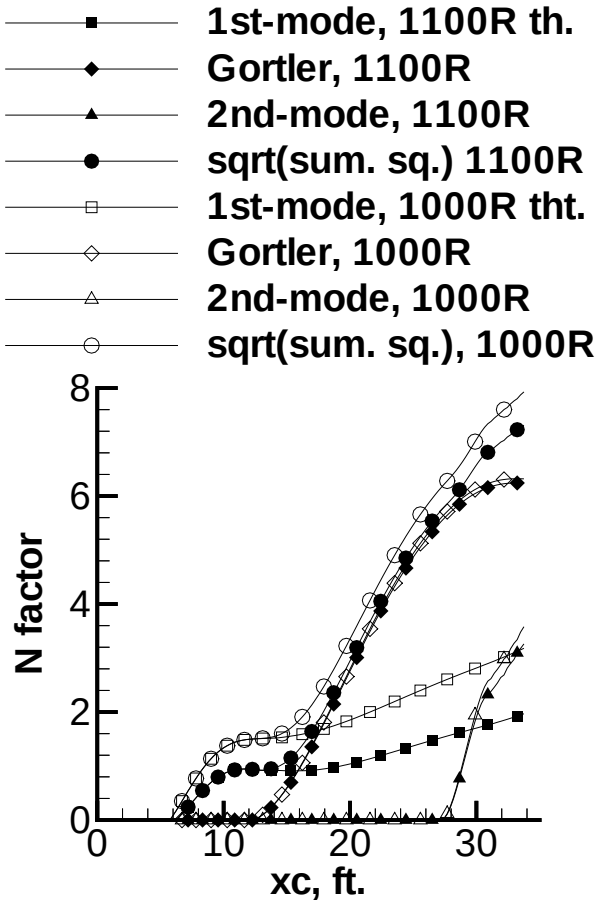

Figure 21: Effect of Two Different Constant-Temperature Throat and Exit Heating Distributions (i4,i5)

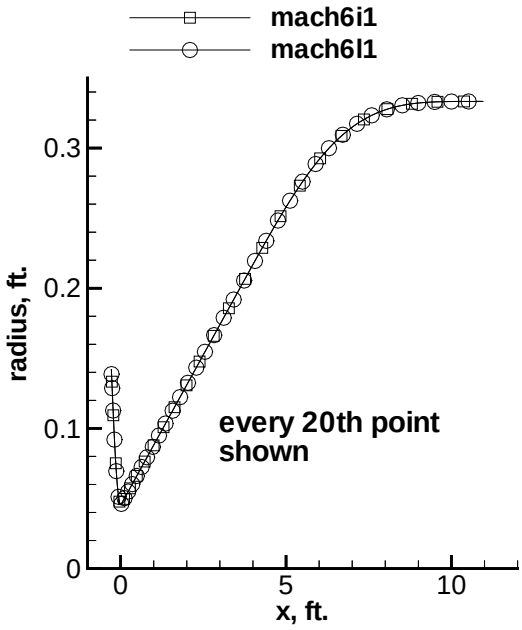

Figure 22: Validation of Very Long Nozzle Results Using Finer Grid (i1,l1)

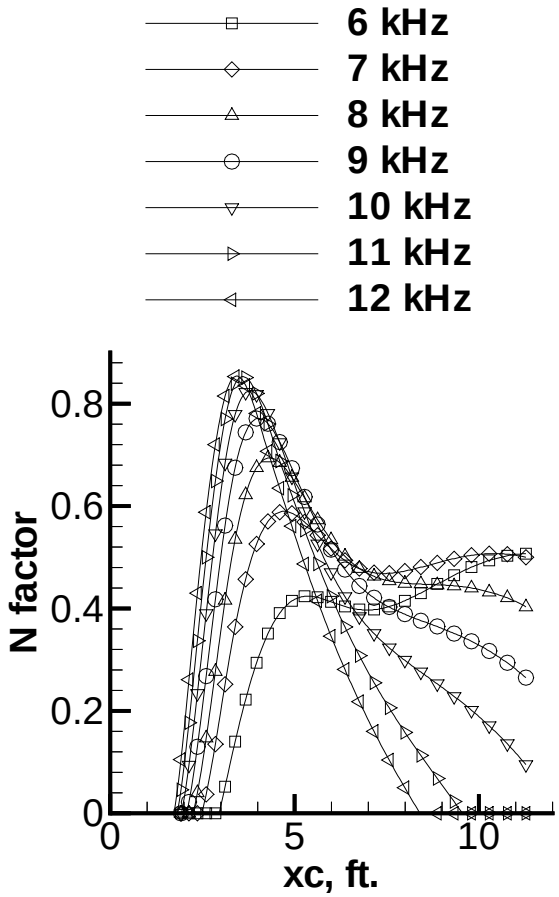

Figure 23: 1st-mode Waves in Heated Throat of Very Long Nozzle (l1)

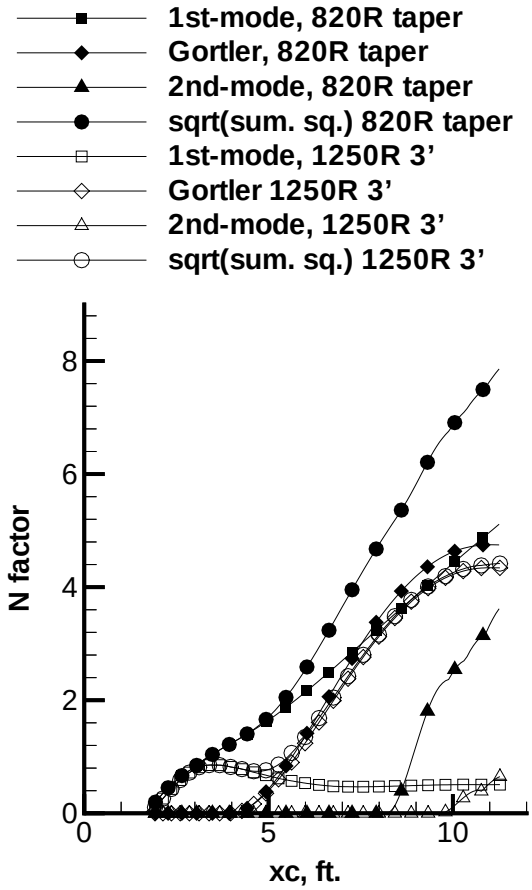

Figure 24: Effect of Throat Heating in Very Long Nozzle (i1,l1)

in excess of 40 cpu hours to compute, on a 167 MHz Sun Ultrasparc 1 cpu. The majority of this time is spent marching downstream looking for the first point of instability. Although CPU time can be decreased if the user makes multiple runs hunting for the first point of instability, this requires more labor. An automated method of selecting frequencies and streamwise positions is needed, to reduce the CPU time spent looking for the first instability at each frequency.

Figure 24 reiterates the effect of throat heating on the N-factor envelopes. Case `i1` has an 820R throat temperature which tapers to 540R at the exit, and the lower grid resolution. Case `l1` maintains a 1250R throat temperature for the first 3 feet of arc length, followed by a linear taper to 540R at the exit. Both nozzles have 8-inch inviscid exit diameters and are operated at $P_t = 150$ psia and $T_t = 820$ Rankine. The first mode N-factor decreases from 5.1 to 0.5 at the exit, due to the heating. The second mode also decreases with heating. The Görtler instability decreases slightly. The combination again shows the dramatic improvement seen earlier.

Figure 25 shows the effect of grid resolution on the 1st-mode waves. Case `l2` has 398 boundary-layer profile stations downstream of the throat; the e^N computations were carried out between stations 186 and 398. Case `i3` has 254 profile stations downstream of the throat, and the e^N computations were carried out between stations 112 and 254. Both cases have the high 1250R throat temperature, maintained for 3 feet, followed by a linear decrease to 540R at the exit. Both have 24-inch inviscid exit diameters and are operated at $P_t = 150$ psia and $T_t = 820$ Rankine. The most-amplified frequencies agree in N-factor to about 0.5%. The data for the 2 kHz

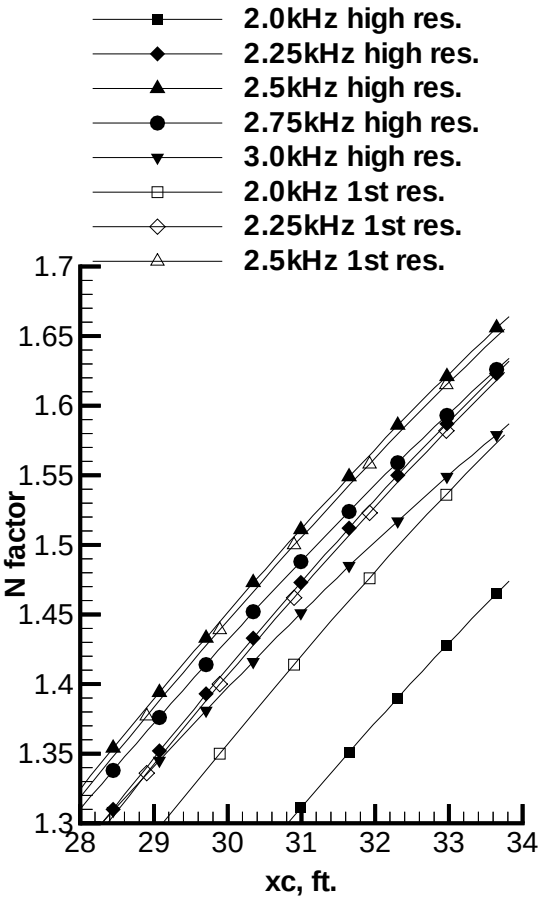

Figure 25: Effect of Resolution on 1st-Mode Waves (l2,i3)

waves differ by about 10%, but this does not affect the results which are based on the most amplified frequencies. Every 5th point is shown.

Figure 26 shows the effect of resolution on the 2nd-mode waves, for the same two cases. Every 5th point is plotted. The repeated frequencies agree to within about 1%, at the most amplified frequency. Figure 27 shows the effect of resolution on the Görtler waves. The two cases agree to within about 0.05%, at the most amplified frequency.

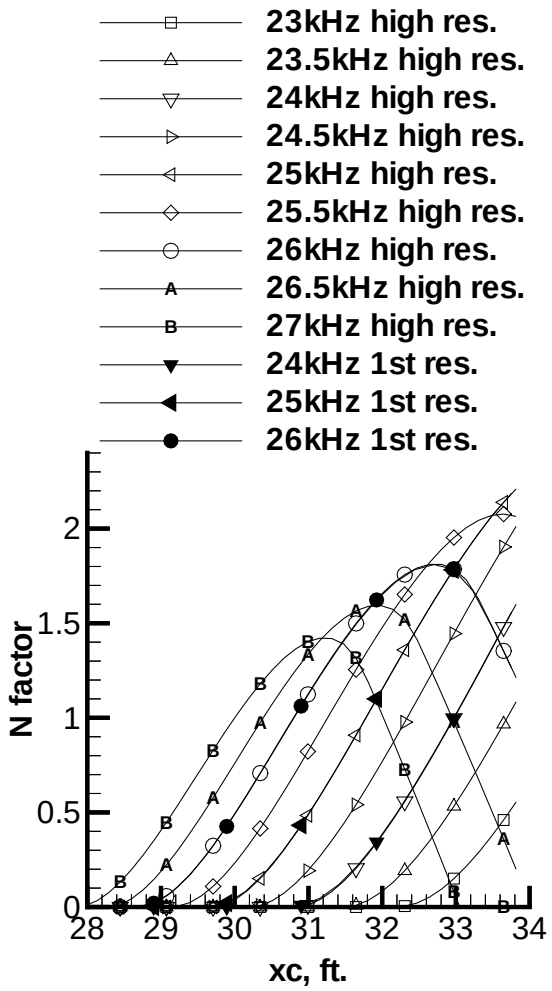

Figure 26: Effect of Resolution on 2nd-Mode Waves (l2,i3)

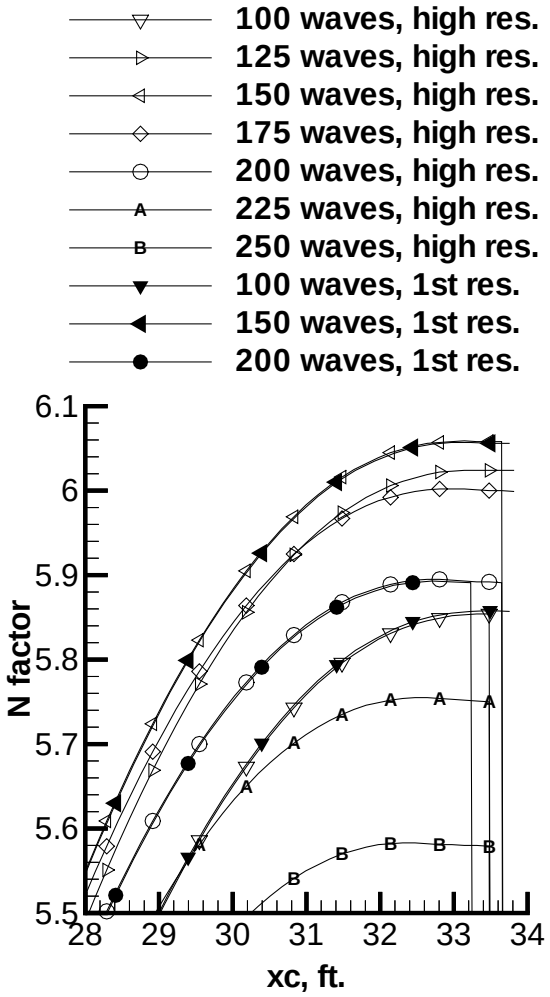

Figure 27: Effect of Resolution on Görtler Waves (l2,i3)

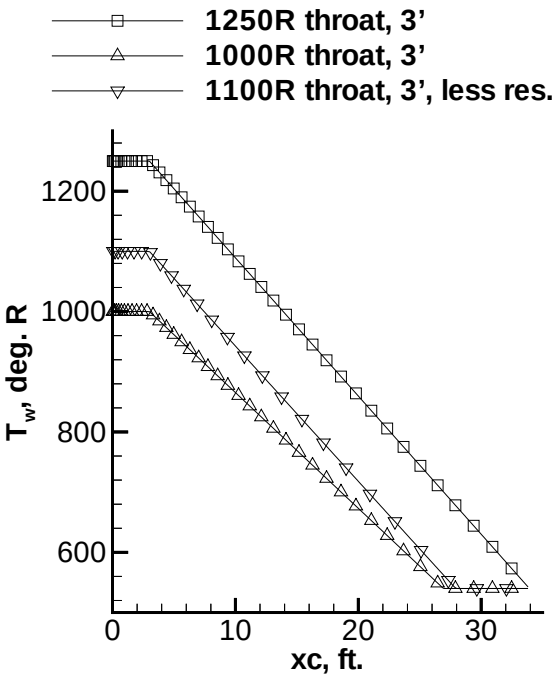

Figure 28: Three Temperature Distributions in Very Long Nozzle (l2,l3,i4)

Further Effects of Temperature Distribution in the 24-inch Full-Scale Nozzle

Figure 28 shows 3 wall-temperature distributions used for further computations in the full-scale version of the very long nozzle with high resolution. These nozzles have a 24-inch inviscid exit diameter and are about 33 feet long. All the cases were computed at $P_t = 150$ psia and $T_t = 820$ Rankine. Case `l2` has a throat heated to 1250R for the first 3 feet of arc length, followed by a linear decrease in isothermal wall temperature to 820R at the exit. Case `l3` is heated only to 1000R at the throat, again for the first 3 feet, followed by a linear decrease to 540R at 6 feet upstream of the exit. The last 7 feet is held at room temperature to eliminate thermal-stress effects in the window area. Case `i4` has the earlier lesser resolution and an intermediate throat temperature.

Figure 29 shows the N-factor envelopes for the 3 cases. The filled and unfilled diamonds and the 'B' symbols show the Görtler envelope. The effect of heating is small. The effect on the 2nd-mode is significant, with the hottest throat and the largest temperature gradient again associated with the weakest

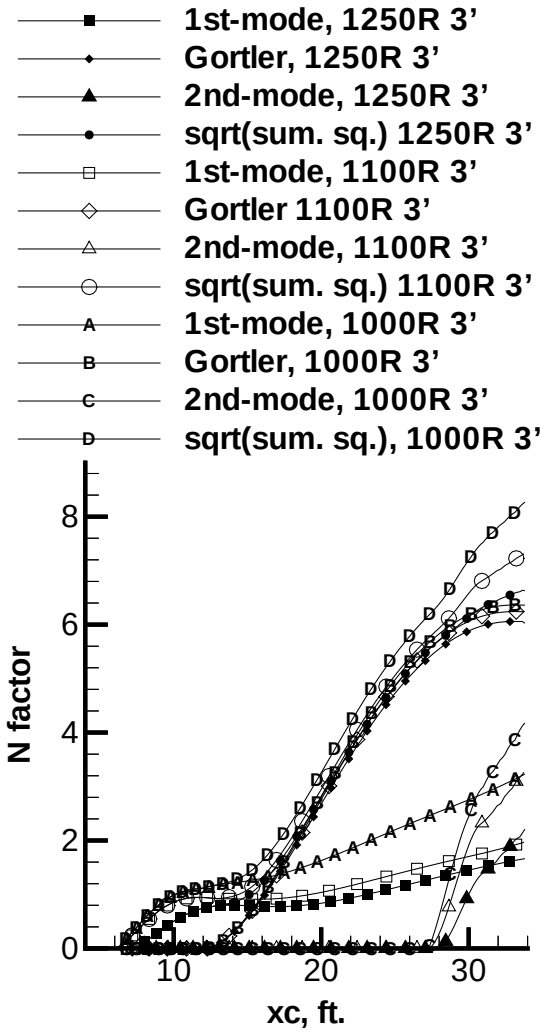

Figure 29: N-Factors for Three Temperature Distributions in Very Long Nozzle (l2,l3,i4)

2nd-mode waves, for unknown reasons. The effect on the 1st mode is nearly the same for the two cases with the hotter throats, while the 3rd case with the 1000R throat has significantly larger growth. Key parameters are again summarized in Table 4. With sufficient heating at the nozzle throat, the boundary layer is predicted to be laminar to the nozzle exit. A smaller throat temperature results in more growth and earlier transition.

Results at and Near
Final Design Point for Prototype

An inviscid exit diameter of 9.0 inches was selected for the prototype. This is a closer match to the inside diameter of commonly available thick-

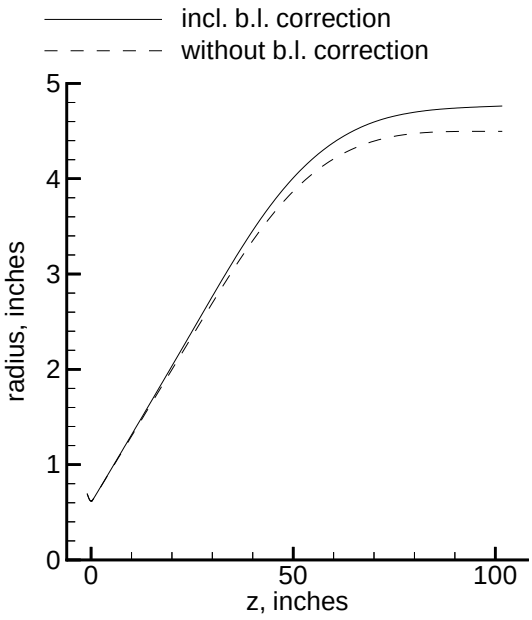

Figure 30: Contour for Prototype Nozzle (m1)

walled pipe, which can be used to fabricate some of the nozzle parts. It also should allow the use of the same models used in the open-jet 7.5-inch nozzle at Langley. Since this prototype has an intermediate Reynolds number compared to the cases computed previously, further studies were carried out to determine an optimum length and the required throat temperatures. Greater detail is shown for the computations for this case, since actual fabrication is planned.

Figure 30 shows the contour of the final design for the prototype nozzle, which has an inviscid exit diameter of 9.0 inches and a length of about 8.5 feet. Details of the inviscid contour are shown in Table 1. The relative length of the nozzle is less than that of the full-scale version because larger curvature is allowable at the lower Reynolds number. The correction due to displacement thickness is also shown in Figure 30; this thickness is about 1/4-inch at the nozzle exit.

Figure 31 shows the 1st-mode N-factors computed in this prototype nozzle at a total pressure of 150 psia and a total temperature of 820R. The wall temperature is held at 1000R for the first 1.0 feet of arclength, and then decreases linearly to 540R, where it is held for the last 2 feet of arclength. There are 201 grid points in the boundary-layer computation normal to the wall, and 690 in the streamwise direction. Some 344 boundary layer profiles are sup-

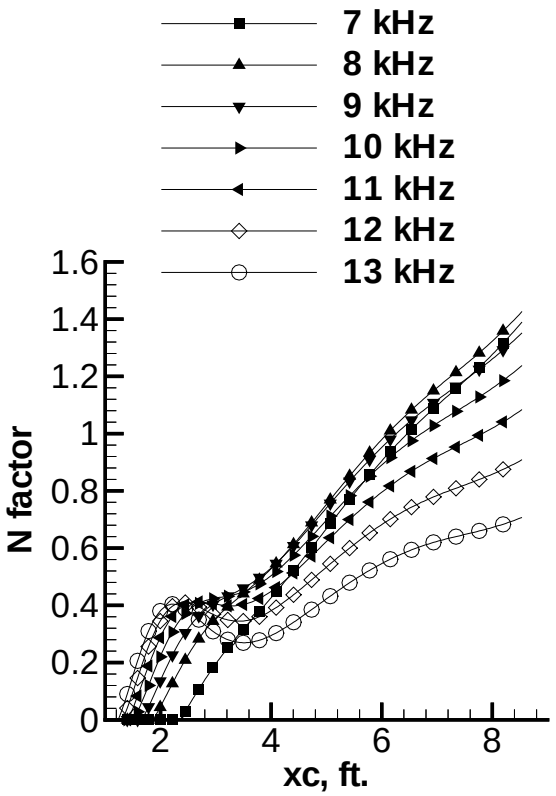

Figure 31: 1st-Mode N factors in Prototype Nozzle at $P_t = 150$ psia and $T_t = 820$R (m1)

plied to the e^{Malik} code for the N-factor computations. The lower frequencies begin to amplify farther downstream, with the intermediate frequencies showing the most amplification at the nozzle exit.

Figure 32 shows the wave angles computed for these 1st-mode waves. e^{Malik} is set to allow the wave angles to vary at each frequency in order to find the most-amplified wave. Amplification is first found at a wave angle of about 74 degrees, after which the wave angle decreases to 55-65 degrees at the exit. A smooth variation is observed through the accelerating and cooling boundary layer.

Figure 33 shows the N factors computed for 2nd-mode waves in the nozzle. At the exit, the most amplified frequency is about 47 kHz, and the N factor is 1.7, still small. These waves are identified by their zero wave angles.

Figure 34 shows the Görtler N factors. As in all the other cases, these were computed assuming a fixed number of waves around the nozzle circumference, as in Chen [22]. The case with 300 waves

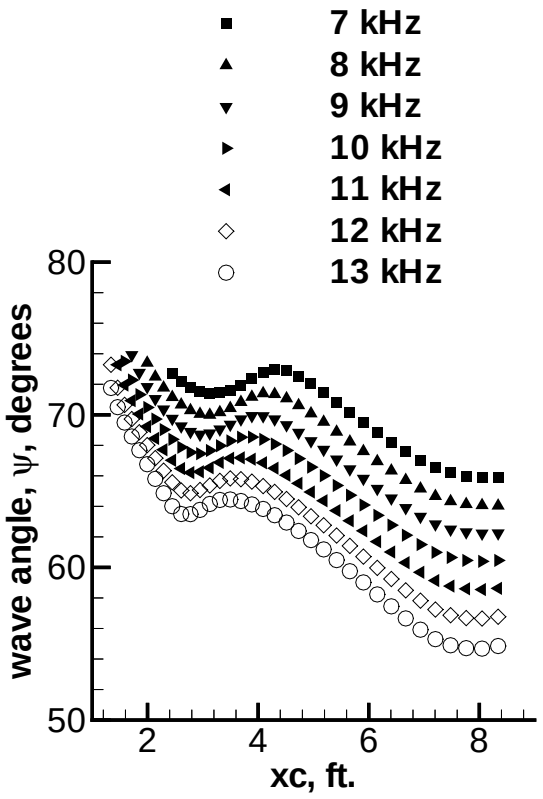

Figure 32: 1st-Mode Wave Angles in Prototype Nozzle at $P_t = 150$ psia and $T_t = 820$R (m1)

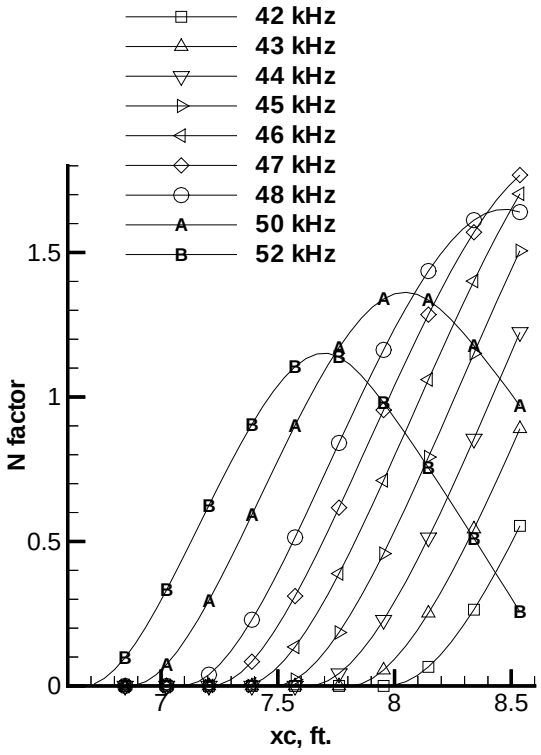

Figure 33: 2nd-Mode N factors in Prototype Nozzle at $P_t = 150$ psia and $T_t = 820$R (m1)

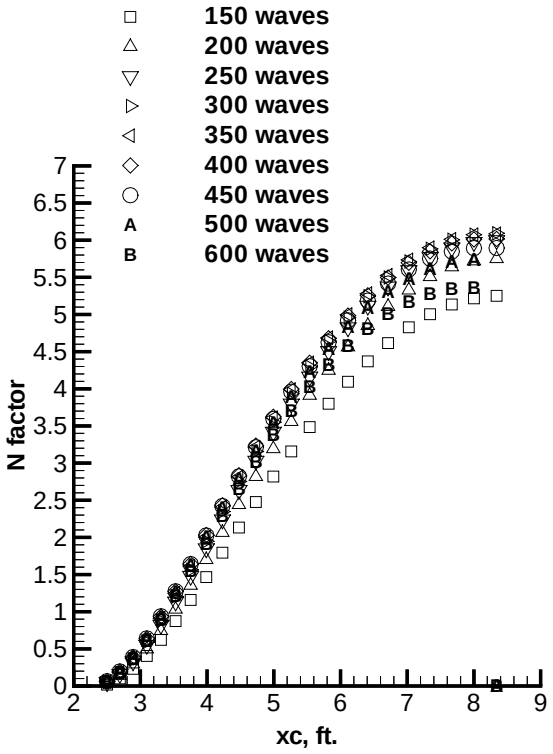

Figure 34: Görtler N factors in Prototype Nozzle at $P_t = 150$ psia and $T_t = 820$R (m1)

around the circumference has the most amplification, reaching an N factor of 6.1 at the exit. Figure 35 shows the wavenumbers β at the various streamwise stations. Here, β is the nondimensional wavenumber, which according to Reference [40] is nondimensionalized using the length $\nu_e x/u_e$. These increase monotonically downstream as the boundary layer thickens.

Accurate computation of the radius of curvature is essential to accurate computation of the Görtler instability. Figure 36 shows every 10th point in both the contour and the computed second derivative. The second derivative is computed directly by the Sivells's method-of-characteristics code, resulting in excellent smoothness. Figure 37 shows a detail of the contour and the radius of curvature in the critical region where the concave curvature is largest. The radius of curvature is computed both from the Sivell's code second derivatives, and via 2nd-order interpolation from these. Every 2nd point is plotted. A small amount of waviness is evident in the interpolated radii. This causes a small amount of waviness

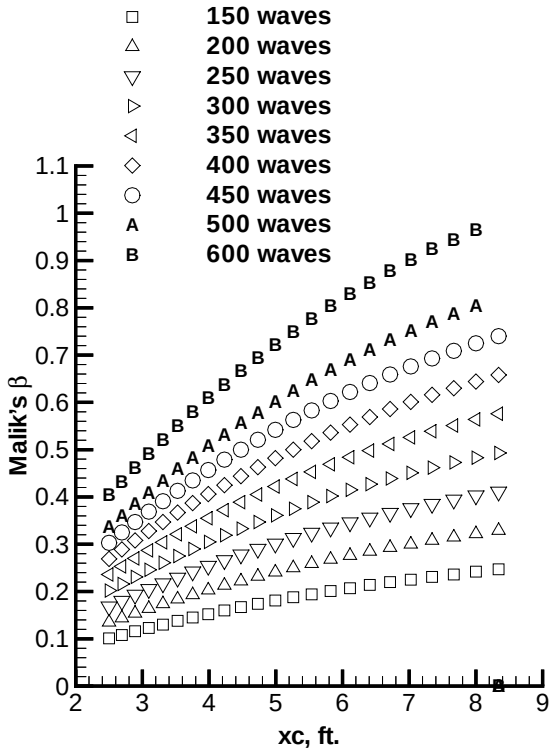

Figure 35: Görtler Wavenumbers in Prototype Nozzle at $P_t = 150$ psia and $T_t = 820$R (m1)

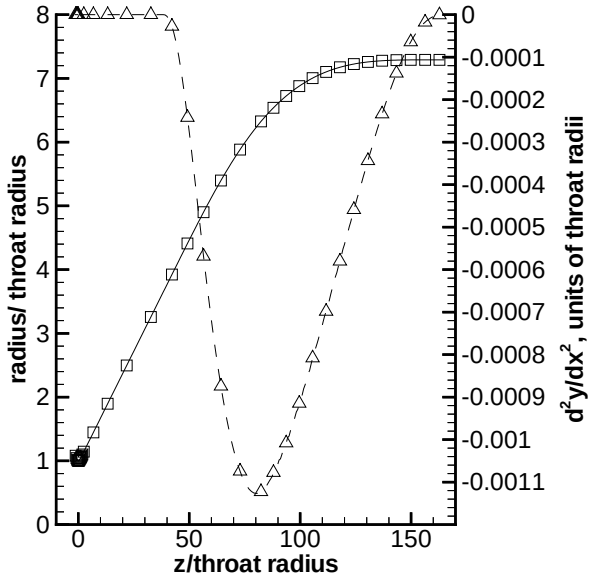

Figure 36: Contour and 2nd Derivative for Prototype Nozzle (m1)

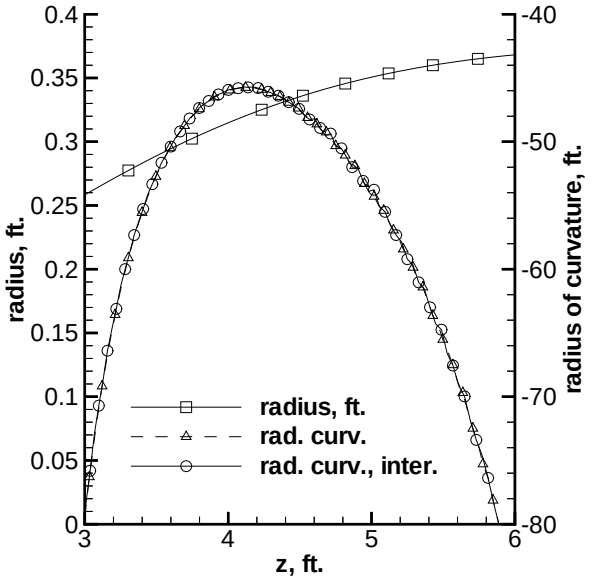

Figure 37: Contour and Radius of Curvature for Prototype Nozzle (m1)

in the Görtler N factors. However, the waviness in both cases has been reduced to the point where it is barely noticeable.

Accurate computation of the boundary layer profiles is also essential, especially near the boundary layer edge where the critical layer is. Although earlier computations (`g1,g2`) showed that N factors computed with 101 and 201 wall-normal points agreed to within less than 0.5%, 201 points were used in all the computations shown in this paper. Figure 38 shows profiles of the slopes of the velocity and temperature profiles, at an arclength position 0.5003 ft. downstream of the bleed lip tip, near the throat. All points are shown. The resolution of the boundary layer edge is good. FZ and TZ are nondimensional transformed derivatives of the velocity and temperature profiles [27, Eqn. (23,25)]. Figure 39 shows similar results near the nozzle exit. Good resolution is again present.

Roughness is a critical issue for these nozzles, especially near the throat. Here, allowable peak roughness is computed using the $Re_k = 12$ criterion proposed by Beckwith [4]. Although this criterion is valid only near the throat, where the Mach number is low, it also presents a lower bound farther downstream. Figure 40 shows the results for 4 wall temperature distributions. In all cases, the stagnation temperature is 820R, and in the first three cases, the stagnation pressure is 150 psia. Case `m1` has a 1000R

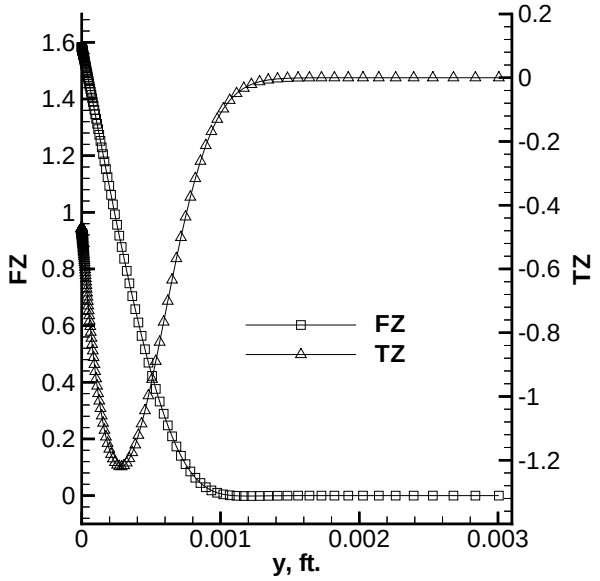

Figure 38: Slopes of Non-Dimensional Velocity and Temperature Profiles near Throat at $s = 0.5003$ ft. (m1)

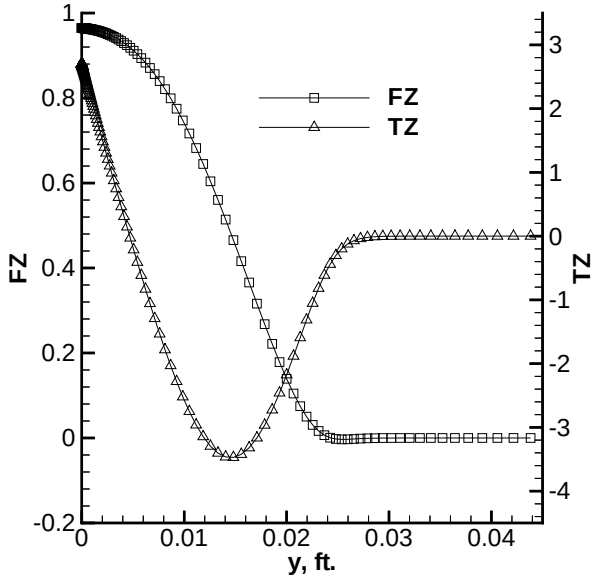

Figure 39: Slopes of Non-Dimensional Velocity and Temperature Profiles near Exit at $s = 7.0242$ ft. (m1)

throat for the first 1 foot of arclength, followed by a linear taper to 540R, where the last 2 feet is held. Case `m2` has a linearly tapering isothermal temperature from 820R at the bleed lip tip to 540R at the exit. Case `m3` has an isothermal wall that is 820R over the whole nozzle. Case `m4` is the same as `m1`, except that the pressure is raised to 200 psia. Even with this strict criterion, the allowable peak roughness for the downstream half of the nozzle is more than 0.010 inches for all 4 cases. This shows that in this region the joints between nozzle sections and with the windows will not be that difficult to implement. The edge Mach number is also shown in the figure, and is the same for all cases; the high Mach number present in the downstream half of the nozzle shows in this region the $Re_k = 12$ criterion is conservative by an order of magnitude or more [13].

The nozzle throat is a different matter. Figure 41 shows a detail of the allowable roughness in the first half of the nozzle. A long nozzle of this type must be constructed in sections. If the first joint is placed at 10 inches, the allowable step is less than 0.001 inches, which will be difficult to achieve and maintain, particularly given the thermal stresses present. Figure 42 shows a 2nd detail in the bleed lip region. The higher temperature at 150 psi increases the allowable roughness by about 23% in the main part of the bleed lip. The higher wall temperature decreases the density near the wall and thus increases the allowable roughness for a fixed roughness Reynolds number. An increase in pressure from 150 to 200 psia almost cancels the effect of an increase in temperature from 820 to 1000R. The peak values are roughly 70 microinches; if we use Beckwith's rule of thumb to convert to the rms values specified to machine shops, a value of about 1-2 microinches rms is needed [4]. This is not easy to achieve without large flaws. The first 0.05 inches of the bleed lip indicates a much tighter requirement, but perhaps this region is relatively stable since the boundary-layer Reynolds number is small here.

Figure 43 shows the N-factor envelopes in the prototype nozzle at $P_t = 150$ psia and $T_t = 820$ R, for the three different wall temperature distributions described above. Key parameters are shown in Table 5. For the first case, which is the nominal design, N_{tot} never reaches 7.5. Transition is assumed at the nozzle exit, for the purpose of computing the numbers in the table. The forward-pointing cone that ends at the nozzle exit and is bounded by the uniform-flow Mach-6 lines upstream will be the part of the quiet flow that is generally useful. This has

ID	$N = 6.5$	$N = 7.5$	Re_{quiet}	D_q	L_q
m1	$xc = 8.5$ ft.	past exit	13.2 million	0.72 ft.	4.3 ft.
m2	$xc = 6.5$ ft.	$xc = 7.4$ ft.	10.2 million	0.56 ft.	3.3 ft.
m3	$xc = 6.0$ ft.	$xc = 6.8$ ft.	8.1 million	0.44 ft.	2.6 ft.

Table 5: Quiet Reynolds Number vs. Wall Temperature for the Prototype 9-inch Nozzle

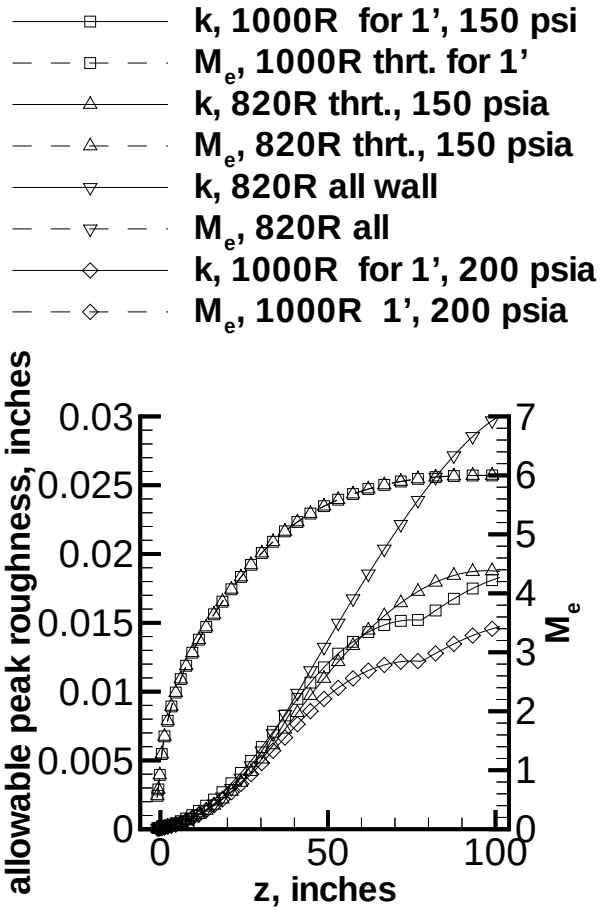

Figure 40: Allowable Peak Roughness for $Re_k = 12$ in Prototype Nozzle at Four Operating Conditions (m1,m2,m3,m4)

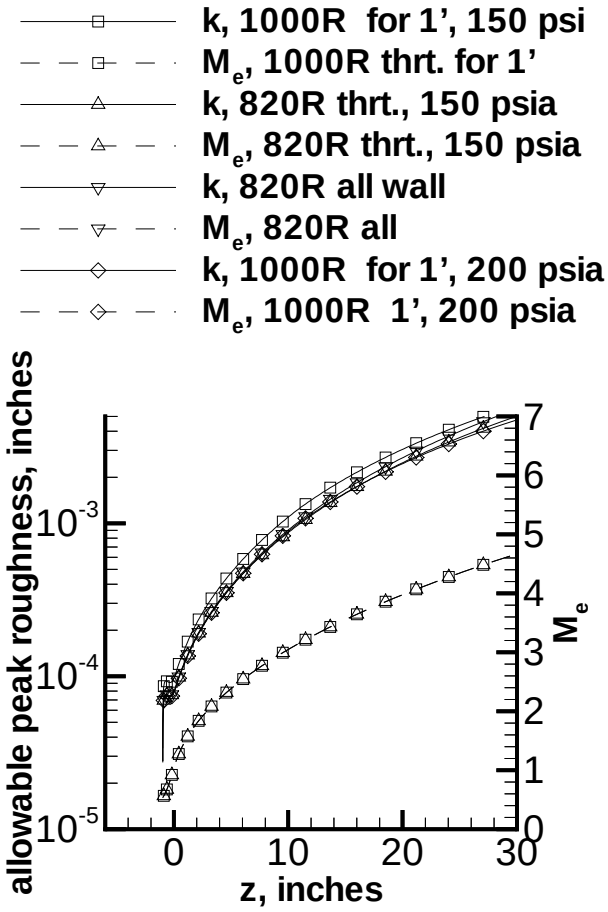

Figure 41: Detail of Allowable Peak Roughness for $Re_k = 12$ in Prototype Nozzle at Four Operating Conditions (m1,m2,m3,m4)

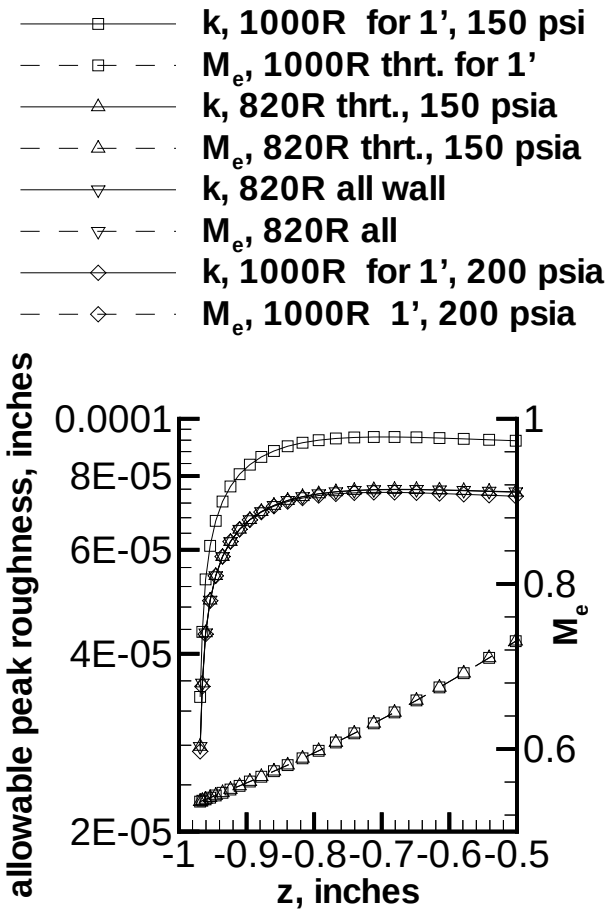

Figure 42: Bleed Lip Detail of Allowable Peak Roughness for $Re_k = 12$ in Prototype Nozzle at Four Operating Conditions (m1,m2,m3,m4)

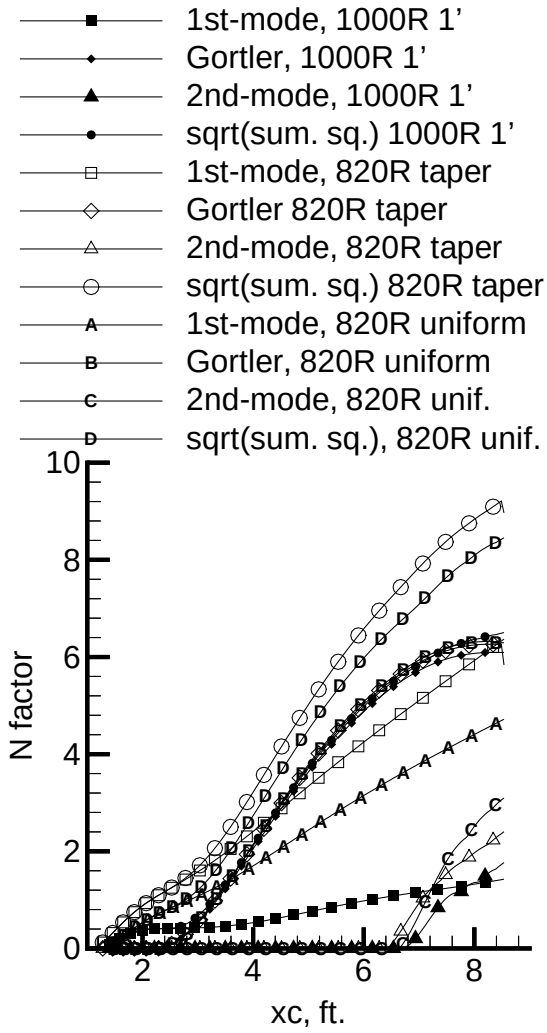

Figure 43: N-factor Envelopes for Prototype Nozzle at $P_t = 150$ psia, $T_t = 820$R and Three Wall Temperature Distributions (m1,m2,m3)

a length of 2.15 ft., a diameter of 0.72 ft., and a Reynolds number of 6.6 million.

The second and third cases with smaller throat temperatures have dramatically reduced performance. Clearly, some throat heating is essential to successful operation of the nozzle, as is the requirement for the temperature to decrease with streamwise distance.

Summary

Using e^N methods, a 24-inch Mach-6 nozzle is designed to remain quiet to a length Reynolds number in excess of 36 million. Lengthening the nozzle re-

duces the Görtler N factor, although it does not reduce the Görtler number. The nozzle-wall temperature is maintained higher than T_t near the throat, and it made to decrease to ambient near the exit. This temperature distribution greatly reduces the growth of 1st and 2nd-mode instabilities. The reduction in the growth of the first mode was expected, but the reduction in the growth of the second mode remains to be explained. The two factors must be combined carefully to be effective.

Roughness effects are controlled by limiting the maximum pressure, and by obtaining a high polish in the throat. The high mass flow is affordable due to a short runtime (1 sec.). The Ludwieg tube design is proven both to maintain quiet flow and to be workable for stability and transition experiments.

A 9-inch prototype is also designed, and should remain quiet to a length Reynolds number in excess of 13 million, according to similar e^N computations. This performance would be twice that of the best nozzle yet tested at hypersonic speeds. Construction of the 9-inch prototype should be completed in late 1998.

Funding for the 24-inch full-scale tunnel has yet to be identified. The computations suggest that an even larger tunnel with yet higher quiet Reynolds number should be possible using the combination of length and throat heating.

Acknowledgements

The work is funded by AFOSR under grant F49620-97-1-0037, originally monitored by Len Sakell and now monitored by Steve Walker. The generous cooperation of the NASA Langley quiet tunnel group is appreciated. The 8-year effort that comes to a milestone in this paper would not have been successful without the suggestions and encouragement of Ivan Beckwith, Dennis Bushnell, Frank Chen, Len Sakell, Steve Wilkinson, and others. Matching funds for tunnel construction are provided by a gift from the Boeing Company.

REFERENCES

[1] AGARD, editor. *Sustained Hypersonic Flight*. AGARD, April 1997. CP-600, vol. 3.

[2] Timothy Alcenius, S.P. Schneider, Ivan E. Beckwith, and John J. Korte. Development of square nozzles for high-speed low-disturbance wind tunnels. Paper 94-2578, AIAA, June 1994.

[3] Timothy Alcenius and Steven P. Schneider. Development of a code for wall contour design in the transonic region of axisymmetric and square nozzles. Contractor Report CR-194857, NASA, January 1994.

[4] I. Beckwith, F. Chen, S. Wilkinson, M. Malik, and D. Tuttle. Design and operational features of low-disturbance wind tunnels at NASA Langley for Mach numbers from 3.5 to 18. Paper 90-1391, AIAA, June 1990.

[5] I.E. Beckwith, F.J. Chen, and T.R. Creel. Design requirements for the NASA Langley supersonic low-disturbance wind tunnel. Paper 86-0763, AIAA, 1986.

[6] I.E. Beckwith, F.J. Chen, and M.R. Malik. Transition research in the Mach-3.5 low-disturbance wind tunnel and comparisons of data with theory. Technical Report TP 892379, Society of Automotive Engineers, 1989.

[7] I.E. Beckwith and B.B. Holley. Görtler vortices and transition in wall boundary layers of two Mach-5 nozzles. Technical Paper 1869, NASA, 1981.

[8] I.E. Beckwith and C.G. Miller III. Aerothermodynamics and transition in high-speed wind tunnels at NASA Langley. *Annual Review of Fluid Mechanics*, 22:419–439, 1990.

[9] I.E. Beckwith and W.O. Moore III. Mean flow and noise measurements in a Mach-3.5 pilot quiet tunnel. Paper 82-0569, AIAA, March 1982.

[10] Alan E. Blanchard, Jason T. Lachowicz, and Stephen P. Wilkinson. Performance of the NASA-Langley Mach-6 quiet wind tunnel. Paper 96-0441, AIAA, January 1996.

[11] Alan E. Blanchard, Jason T. Lachowicz, and Stephen P. Wilkinson. NASA Langley Mach 6 quiet wind-tunnel performance. *AIAA Journal*, 35(1):23–28, January 1997.

[12] S. A. Bouslog, M. Y. An, L.N. Hartmann, and S. M. Derry. Review of boundary layer transition flight data on the space shuttle orbiter. Paper 91-0741, AIAA, January 1991.

[13] Albert L. Braslow. A review of factors affecting boundary-layer transition. TN D-3384, NASA, August 1966.

[14] D. M. Bushnell. Notes on initial disturbance fields for the transition problem. In M. Y. Hussaini and R.G. Voigt, editors, *Instability and Transition, Volume I*, pages 217–232, Berlin, 1990. Springer-Verlag. Materials of the workshop held May 15 – June 9,1989 in Hampton, Virginia.

[15] A.J. Cable and R.N. Cox. The Ludwieg pressure-tube supersonic wind tunnel. *Aeronautical Quarterly*, 14:143–157, 1963.

[16] L.N. Cattafesta, V. Iyer, J.A. Masad, R.A. King, and J.R. Dagenhart. Three-dimensional boundary-layer transition on a swept wing at Mach 3.5. *AIAA Journal*, 33(11):2032–2037, November 1995.

[17] F.-J. Chen, M.R. Malik, and I.E. Beckwith. Boundary-layer transition on a cone and flat plate at Mach 3.5. *AIAA Journal*, 27(6):687–693, 1989.

[18] F. J. Chen and S. P. Wilkinson. Design of Mach 2.4 quiet nozzles for the NASA Langley supersonic low-disturbance pilot tunnel. Paper 94-2506, AIAA, June 1994.

[19] F.J. Chen. Boundary-layer transition extent measurements on a cone and flat plate at Mach 3.5. Paper 93-0342, AIAA, January 1993.

[20] F.J. Chen, I.E. Beckwith, and T.R. Creel. Effects of streamwise variations in noise levels and spectra on supersonic boundary-layer transition. Paper 84-0010, AIAA, January 1984.

[21] F.J. Chen, M.R. Malik, and I.E. Beckwith. Advanced Mach-3.5 axisymmetric quiet nozzle. Paper 90-1592, AIAA, June 1990.

[22] F.J. Chen, S.P. Wilkinson, and I.E. Beckwith. Görtler instability and hypersonic quiet nozzle design. Paper 91-1648, AIAA, June 1991.

[23] Anthony Demetriades. Stabilization of a nozzle boundary layer by local surface heating. *AIAA Journal*, 34(12):2490–2495, 1996.

[24] J.I. Erdos and R. Bakos. Prospects for a quiet hypervelocity shock-expansion tunnel. Paper 94-2500, AIAA, June 1994.

[25] C.R. Fitch. Flow quality improvement at Mach 8 in the VKF 50-inch hypersonic wind tunnel B. Technical Report AEDC-TR-66-82, Arnold Engineering Development Center, 1966.

[26] J.M. Floryan. On the Görtler instability of boundary layers. *Progress in Aerospace Sciences*, 28:235–271, 1991.

[27] J.E. Harris and D.K. Blanchard. Computer program for solving laminar, transitional, or turbulent compressible boundary-layer equations for two-dimensional and axisymmetric flow. Technical Report NASA-TM-83207, NASA, February 1982.

[28] W.D. Harvey, P.C. Stainback, J.B. Anders, and A.M. Cary. Nozzle wall boundary-layer transition and freestream disturbances at Mach 5. *AIAA Journal*, 13(3):307–314, 1975.

[29] Th. Herbert. Secondary instability of boundary layers. *Annual Reviews of Fluid Mechanics*, 20:487–526, 1988.

[30] Th. Herbert. Boundary-layer transition - analysis and prediction revisited. Paper 91-0737, AIAA, Jan. 1991.

[31] Th. Herbert. Parabolized stability equations. In *AGARD Report 793, Special Course on* Progress in Transition Modelling, pages 4/1 – 4/34, 1994.

[32] Uwe G. Hingst. Laminar/turbulent flow transition effects on high speed missile domes. In *CP-493, Missile Aerodynamics*, pages 27–1 to 27–8. AGARD, 1990.

[33] R.A. King. Three-dimensional boundary-layer transition on a cone at Mach 3.5. *Experiments in Fluids*, 13(5):305–314, 1992.

[34] L. Kleiser and T. Zang. Numerical simulation of transition in wall-bounded shear flows. *Annual Reviews of Fluid Mechanics*, 23:495–537, 1991.

[35] H.A. Korejwo and M.S. Holden. Ground test facilities for aerothermal and aero-optical evaluation of hypersonic interceptors. Paper 92-1074, AIAA, February 1992.

[36] Dale W. Ladoon, John D. Schmisseur, and Steven P. Schneider. Laser-induced resonance in a forward-facing cavity at Mach 4. Paper 97-0339, AIAA, January 1997.

[37] Dale W. Ladoon and Steven P. Schneider. Stability and transition experiments on an elliptic cone at Mach 4 using an electrical-discharge perturber. In *3rd Symposium on Transition and Turbulent Compressible Flows*. ASME Fluid Engineering Division, June 1997.

[38] L. M. Mack. Boundary layer linear stability theory. In *Report 709, Special Course on Stability and Transition of Laminar Flow*, pages 1–81. AGARD, March 1984.

[39] M.R. Malik. Numerical methods for hypersonic boundary layer stability. *Journal of Computational Physics*, 86:376–413, 1990.

[40] Mujeeb R. Malik. e**Malik: A new spatial stability analysis program for transition prediction using the e**N method. Technical Report HTC-8902, High Technology Corporation, March 1989. See also HTC-9203, which is almost identical.

[41] Mujeeb R. Malik. Prediction and control of transition in supersonic and hypersonic boundary layers. *AIAA Journal*, 27(11):1487–1493, November 1989.

[42] J.A. Masad and A.H. Nayfeh. Laminar flow control of subsonic boundary layers by suction and heat-transfer strips. *Physics of Fluids A*, 4(6):1259–1272, June 1992.

[43] E.L. Morrisette, T.R. Creel, and F.J. Chen. Effects of cone surface waviness on transition in quiet and noisy supersonic freestreams. Paper 86-1086, AIAA, May 1986.

[44] Scott Edward Munro. Effects of elevated driver-tube temperature on the extent of quiet flow in the Purdue Ludwieg tube. Master's thesis, School of Aeronautics and Astronautics, Purdue University, December 1996. Available from the Defense Technical Information Center as AD-A315654.

[45] R. Narasimha. The laminar-turbulent transition zone in the turbulent boundary layer. *Progress in Aerospace Science*, 22:29–80, 1985.

[46] E. Piltz. Boundary-layer effects on pressure variations in Ludwieg tubes. *AIAA Journal*, 10:1095–1097, 1972.

[47] A. Pope and K. Goin. *High-Speed Wind Tunnel Testing*. Wiley, New York, 1965.

[48] H. Reed, R. Kimmel, D. Arnal, and S. Schneider. Drag prediction and transition in hypersonic flow. In *Sustained Hypersonic Flight*. AGARD, April 1997. Paper C15 in CP-600, vol. 3. Also appears as AIAA Paper 97-1818, June 1997.

[49] H.L. Reed and W.S. Saric. Stability of three-dimensional boundary layers. *Annual Review of Fluid Mechanics*, 21:235–284, 1989.

[50] Eli Reshotko. Boundary layer instability, transition, and control. Paper 94-0001, AIAA, January 1994. The 1994 Dryden Lecture in Research.

[51] D.A. Russell, G.S. Knoke, and J.C. Wai. Uniformity of Ludwieg tube flows. In *Modern Developments in Shock Tube Research, Proceedings of the 10th International Shock Tube Symposium, Kyoto*, pages 244–251, 1975.

[52] Norman E. Scaggs and Kenneth F. Stetson. Boundary layer transition experiments off tunnel centerline. Technical report, Aeromechanics Division, Air Force Wright Aeronautical Labs, 1978. Presented at the 50th semi-annual meeting of the Supersonic Tunnel Association, University of Illinois, 20-22 Sept. 1978.

[53] J.D. Schmisseur, S.P. Schneider, T.R. Salyer, and S.H. Collicott. A repeatable laser-generated localized perturbation for application to fluid mechanics. In the Eight International Symposium on Applications of Laser Techniques to Fluid Mechanics, Lisbon, Portugal, 8-11 July 1996.

[54] S. P. Schneider and C. E. Haven. Quiet-flow Ludwieg tube for high-speed transition research. *AIAA Journal*, 33(4):688–693, April 1995.

[55] Steven P. Schneider. Development of quiet-flow supersonic wind tunnels for laminar-turbulent transition research. Contractor Report CR-197286, NASA, January 1995.

[56] Steven P. Schneider. Design and fabrication of a 9-inch Mach-6 quiet-flow Ludwieg tube. Paper 98-2511, AIAA, June 1998.

[57] Steven P. Schneider. Survey of flight data for boundary-layer transition at hypersonic and supersonic speeds. Paper 98-0432, AIAA, January 1998.

[58] Steven P. Schneider, Steven H. Collicott, J.D. Schmisseur, Dale Ladoon, Laura A. Randall, Scott E. Munro, and T.R. Salyer. Laminar-turbulent transition research in the Purdue Mach-4 quiet-flow Ludwieg tube. Paper 96-2191, AIAA, June 1996.

[59] Steven P. Schneider, Christine E. Haven, Joseph B. McGuire, Steven H. Collicott, Dale Ladoon, and Laura A. Randall. High-speed laminar-turbulent transition research in the Purdue quiet-flow Ludwieg tube. Paper 94-2504, AIAA, June 1994.

[60] G. Schrauf, H. Bieler, and P. Thiede. Transition prediction – the Deutsche Airbus view. In *Proceedings of the First European Forum on Laminar Flow Technology, Hamburg*, pages 73–82, March 16-18, 1992. DGLR-Bericht 92-06.

[61] J.C. Sivells. Aerodynamic design of axisymmetric hypersonic wind-tunnel nozzles. *J. Spacecraft*, 7(11):1292–1299, 1970.

[62] J.C. Sivells. A computer program for the aerodynamic design of axisymmetric and planar nozzles for supersonic and hypersonic wind tunnels. Technical Report AEDC-TR-78-63, Arnold Engineering Development Center, December 1978.

[63] R.F. Starr and C.J. Schueler. Experimental studies of a Ludwieg tube high Reynolds number transonic tunnel. Technical Report AEDC-TR-73-168, Arnold Engineering Development Center, 1973.

[64] Joseph Sternberg. A free-flight investigation of the possibility of high Reynolds number supersonic laminar boundary layers. *J. of the Aeronautical Sciences*, 19(11):721–733, November 1952.

[65] K. F. Stetson and R. L. Kimmel. Example of second-mode instability dominance at a Mach number of 5.2. *AIAA Journal*, 30(12):2974–2976, December 1992.

[66] P.P. Wegener and L.M. Mack. Condensation in supersonic and hypersonic wind tunnels. *Advances in Applied Mechanics*, 5:307–447, 1958.

[67] J.D. Whitfield, C.J. Schueler, and R.F. Starr. High Reynolds number transonic wind tunnels - blowdown or Ludwieg tube? CP 83, AGARD, 1971.

[68] S. P. Wilkinson, S. G. Anders, and F.-J. Chen. Status of Langley quiet flow facility developments. Paper 94-2498, AIAA, June 1994.

[69] S.P. Wilkinson, S.G. Anders, F.-J. Chen, and I.E. Beckwith. Supersonic and hypersonic quiet tunnel technology at NASA Langley. Paper 92-3908, AIAA, July 1992.

[70] R.L. Wright and E.V. Zoby. Flight boundary layer transition measurements on a slender cone at Mach 20. Paper 77-719, AIAA, June 1977.